

# Space is the Place: Effects of Continuous Spatial Structure on Analysis of Population Genetic Data

C.J. Battey<sup>\*,†</sup>, Peter L. Ralph<sup>\*,†</sup> and Andrew D. Kern<sup>\*,†</sup>

<sup>\*</sup>University of Oregon Dept. Biology, Institute for Ecology Evolution

**ABSTRACT** Real geography is continuous, but standard models in population genetics are based on discrete, well-mixed populations. As a result many methods of analyzing genetic data assume that samples are a random draw from a well-mixed population, but are applied to clustered samples from populations that are structured clinally over space. Here we use simulations of populations living in continuous geography to study the impacts of dispersal and sampling strategy on population genetic summary statistics, demographic inference, and genome-wide association studies. We find that most common summary statistics have distributions that differ substantially from that seen in well-mixed populations, especially when Wright's neighborhood size is less than 100 and sampling is spatially clustered. Stepping-stone models reproduce some of these effects, but discretizing the landscape introduces artifacts which in some cases are exacerbated at higher resolutions. The combination of low dispersal and clustered sampling causes demographic inference from the site frequency spectrum to infer more turbulent demographic histories, but averaged results across multiple simulations were surprisingly robust to isolation by distance. We also show that the combination of spatially autocorrelated environments and limited dispersal causes genome-wide association studies to identify spurious signals of genetic association with purely environmentally determined phenotypes, and that this bias is only partially corrected by regressing out principal components of ancestry. Last, we discuss the relevance of our simulation results for inference from genetic variation in real organisms.

**KEYWORDS** Space; Population Structure; Demography; Haplotype block sharing; GWAS

## Introduction

The inescapable reality that biological organisms live, move, and reproduce in continuous geography is usually omitted from population genetic models. However, mates tend to live near to one another and to their offspring, leading to a positive correlation between genetic differentiation and geographic distance. This pattern of “isolation by distance” (Wright 1943) is one of the most widely replicated empirical findings in population genetics (Aguillon *et al.* 2017; Jay *et al.* 2012; Sharbel *et al.* 2000). Despite a long history of analytical work describing the genetics of populations distributed across continuous geography (e.g., Wright (1943); Rousset (1997); Barton *et al.* (2002, 2010); Ringbauer *et al.* (2017); Robledo-Arnuncio and Rousset (2010); Wilkins and Wakeley (2002); Wilkins (2004)), much modern work still describes geographic structure as a set of discrete populations connected by migration (e.g., Wright 1931; Epperson 2003; Rousset and Leblois 2011; Shirk and Cushman 2014; Lundgren and Ralph 2019)

Manuscript compiled: Monday 10<sup>th</sup> February, 2020

<sup>†</sup>301 Pacific Hall, University of Oregon Dept. Biology, Institute for Ecology and Evolution. cbattey2@uoregon.edu.

<sup>†</sup>these authors co-supervised this project

39 or as an average over such discrete models (Petkova *et al.* 2015; Al-Asadi *et al.* 2019). For this reason,  
40 most population genetics statistics are interpreted with reference to discrete, well-mixed populations,  
41 and most empirical papers analyze variation within clusters of genetic variation inferred by programs  
42 like *STRUCTURE* (Pritchard *et al.* 2000) with methods that assume these are randomly mating units.

43 The assumption that populations are “well-mixed” has important implications for downstream  
44 inference of selection and demography. Methods based on the coalescent (Kingman 1982; Wakeley  
45 2009) assume that the sampled individuals are a random draw from a well-mixed population that is  
46 much larger than the sample (Wakeley and Takahashi 2003). The key assumption is that the individuals  
47 of each generation are *exchangeable*, so that there is no correlation between the fate or fecundity of a  
48 parent and that of their offspring (Huillet and Möhle 2011). If dispersal or mate selection is limited by  
49 geographic proximity, this assumption can be violated in many ways. For instance, if mean viability or  
50 fecundity is spatially autocorrelated, then limited geographic dispersal will lead to parent–offspring  
51 correlations. Furthermore, nearby individuals will be more closely related than an average random  
52 pair, so drawing multiple samples from the same area of the landscape will represent a biased sample  
53 of the genetic variation present in the whole population (Städler *et al.* 2009).

54 Two areas in which spatial structure may be particularly important are demographic inference and  
55 genome-wide association studies (GWAS). Previous work has found that discrete population structure  
56 can create false signatures of population bottlenecks when attempting to infer demographic histories  
57 from microsatellite variation (Chikhi *et al.* 2010), statistics summarizing the site frequency spectrum  
58 (SFS) (Ptak and Przeworski 2002; Städler *et al.* 2009; St. Onge *et al.* 2012), or runs of homozygosity in a  
59 single individual (Mazet *et al.* 2015). The increasing availability of whole-genome data has led to the  
60 development of many methods that attempt to infer detailed trajectories of population sizes through  
61 time based on a variety of summaries of genetic data (Liu and Fu 2015; Schiffels and Durbin 2014;  
62 Sheehan *et al.* 2013; Terhorst *et al.* 2016). Because all of these methods assume that the populations  
63 being modeled are approximately randomly mating, they are likely affected by spatial biases in the  
64 genealogy of sampled individuals (Wakeley 1999), which may lead to incorrect inference of population  
65 changes over time (Mazet *et al.* 2015). However, previous investigations of these effects have focused on  
66 discrete rather than continuous space models, and the level of isolation by distance at which inference  
67 of population size trajectories become biased by structure is not well known. Here we test how two  
68 methods suitable for use with large samples of individuals – stairwayplot (Liu and Fu 2015) and  
69 SMC++ (Terhorst *et al.* 2016) – perform when applied to populations evolving in continuous space  
70 with varying sampling strategies and levels of dispersal.

71 Spatial structure is also a major challenge for interpreting the results of genome-wide association  
72 studies (GWAS). This is because many phenotypes of interest have strong geographic differences due  
73 to the (nongenetic) influence of environmental or socioeconomic factors, which can therefore show  
74 spurious correlations with spatially patterned allele frequencies (Bulik-Sullivan *et al.* 2015; Mathieson  
75 and McVean 2012). Indeed, two recent studies found that previous evidence of polygenic selection on  
76 human height in Europe was confounded by subtle population structure (Sohail *et al.* 2018; Berg *et al.*  
77 2018), suggesting that existing methods to correct for population structure in GWAS are insufficient.  
78 However we have little quantitative idea of the population and environmental parameters that can be  
79 expected to lead to biases in GWAS.

80 Last, some of the most basic tools of population genetics are summary statistics like  $F_{IS}$  and  
81 Tajima’s  $D$ , which are often interpreted as reflecting the influence of selection or demography on  
82 sampled populations (Tajima 1989). Statistics like Tajima’s  $D$  are essentially summaries of the site  
83 frequency spectrum, which itself reflects variation in branch lengths and tree structure of the underlying  
84 genealogies of sampled individuals. Geographically limited mate choice distorts the distribution of  
85 these genealogies (Maruyama 1972; Wakeley 1999), which can affect the value of Tajima’s  $D$  (Städler  
86 *et al.* 2009). Similarly, the distribution of tract lengths of identity by state among individuals contains  
87 information about not only historical demography (Harris and Nielsen 2013; Ralph and Coop 2013)  
88 and selection (Garud *et al.* 2015), but also dispersal and mate choice (Ringbauer *et al.* 2017; Baharian  
89 *et al.* 2016). We are particularly keen to examine how such summaries will be affected by models that  
90 incorporate continuous space, both to evaluate the assumptions underlying existing methods and to  
91 identify where the most promising signals of geography lie.

92 To study this, we have implemented an individual-based model in continuous geography that  
93 incorporates overlapping generations, local dispersal of offspring, and density-dependent survival. We  
94 simulate chromosome-scale genomic data in tens of thousands of individuals from parameter regimes  
95 relevant to common subjects of population genetic investigation such as humans and *Drosophila*, and  
96 output the full genealogy and recombination history of all final-generation individuals. We use these  
97 simulations to test how sampling strategy interacts with geographic population structure to cause  
98 systematic variation in population genetic summary statistics typically analyzed assuming discrete  
99 population models. We then examine how the fine-scale spatial structures occurring under limited  
100 dispersal impact demographic inference from the site frequency spectrum. Last, we examine the  
101 impacts of continuous geography on genome-wide association studies (GWAS) and identify regions of  
102 parameter space under which the results from GWAS may be misleading.

## 103 Materials and Methods

### 104 *Modeling Evolution in Continuous Space*

105 The degree to which genetic relationships are geographically correlated depends on the chance that  
106 two geographically nearby individuals are close relatives – in modern terms, by the tension between  
107 migration (the chance that one is descended from a distant location) and coalescence (the chance that  
108 they share a parent). A key early observation by Wright (1946) is that this balance is often nicely  
109 summarized by the “neighborhood size”, defined to be  $N_W = 4\pi\rho\sigma^2$ , where  $\sigma$  is the mean parent-  
110 offspring distance along each of the x and y axes and  $\rho$  is population density (see (Rousset 1997) for  
111 further discussion of parameter definitions in one- and two-dimensional habitats). This can be thought  
112 of as proportional to the average number of potential mates for an individual (those within distance  
113  $2\sigma$ ), or the number of potential parents of a randomly chosen individual. Empirical estimates of  
114 neighborhood size vary hugely across species – even in human populations, estimates range from 40  
115 to over 5,000 depending on the population and method of estimation (Table 1).

116 The first approach to modeling continuously distributed populations was to endow individuals in a  
117 Wright-Fisher model with locations in continuous space. However, since the total size of the population  
118 is constrained, this introduces interactions between arbitrarily distant individuals, which (aside from  
119 being implausible) was shown by Felsenstein (1975) to eventually lead to unrealistic population  
120 clumping if the range is sufficiently large. Another method for modeling spatial populations is to  
121 assume the existence of a grid of discrete randomly mating populations connected by migration, thus  
122 enforcing regular population density by edict. Among many other results drawn from this class of  
123 “lattice” or “stepping stone” models (Epperson 2003), Rousset (1997) showed that the slope of the linear  
124 regression of genetic differentiation ( $F_{ST}$ ) against the logarithm of spatial distance is an estimate of  
125 neighborhood size. Although these grid models may be good approximations of continuous geography  
126 in many situations, they do not model demographic fluctuations, and limit investigation of spatial  
127 structure below the level of the deme, assumptions whose impacts are unknown. An alternative  
128 method for dealing with continuous geography is a new class of coalescent models, the Spatial Lambda  
129 Fleming-Viot models (Barton *et al.* 2010; Kelleher *et al.* 2014).

130 To avoid hard-to-evaluate approximations, we here used forward-time, individual-based simulations  
131 across continuous geographical space. The question of what regulates real populations has a  
132 long history and many answers (e.g., Lloyd 1967; Antonovics and Levin 1980; Crawley 1990), but it is  
133 clear that populations must at some point have density-dependent feedback on population size, or  
134 else they would face eventual extinction or explosion. In the absence of unrealistic global population  
135 regulation, this regulation must be local, and there are many ways to achieve this (Bolker *et al.* 2003). In  
136 our simulations, each individual’s probability of survival is a decreasing function of local population  
137 density, which shifts reproductive output towards low-density regions, and produces total census sizes  
138 that fluctuate around an equilibrium. This also prevents the population clumping seen by Felsenstein  
139 (1975) (Supplemental Figure S1)). Such models have been used extensively in ecological modeling  
140 (Durrett and Levin 1994; Bolker and Pacala 1997; Law *et al.* 2003; Fournier and Méléard 2004; Champer  
141 *et al.* 2019) but rarely in population genetics, where to our knowledge implementations of continuous  
142 space models before their availability through SLiM (Haller and Messer 2019) have focused on a small

143 number of genetic loci (e.g., Slatkin and Barton 1989; Barton *et al.* 2002; Robledo-Arnuncio and Rousset  
 144 2010; Rossine 2014; Jackson and Fahrig 2014), which limits the ability to investigate the impacts of  
 145 continuous space on genome-wide genetic variation as is now routinely sampled from real organisms.  
 146 By simulating chromosome-scale sequence alignments and complete population histories we are able  
 147 to treat our simulations as real populations and replicate the sampling designs and analyses commonly  
 148 conducted on real genomic data.

#### 149 **A Forward-Time Model of Evolution in Continuous Space**

150 We simulated populations using the program SLiM v3.1 (Haller and Messer 2019). Each time step  
 151 consists of three stages: reproduction, dispersal, and mortality. To reduce the parameter space we  
 152 use the same parameter, denoted  $\sigma$ , to modulate the spatial scale of interactions at all three stages  
 153 by adjusting the standard deviation of the corresponding Gaussian functions. As in previous work  
 154 (Rousset 1997),  $\sigma$  is equal to the mean parent-offspring distance along each of the  $x$  and  $y$  axes.

155 At the beginning of the simulation individuals are distributed uniformly at random on a continuous,  
 156 square landscape. Individuals are hermaphroditic, and each time step, each produces a Poisson number  
 157 of offspring with mean  $1/L$ . Offspring disperse a Gaussian-distributed distance away from the parent  
 158 with mean zero and standard deviation  $\sigma$  in both the  $x$  and  $y$  coordinates. Each offspring is produced  
 159 with a mate selected randomly from those within distance  $3\sigma$ , with probability of choosing a neighbor  
 160 at distance  $d$  proportional to  $\exp(-d^2/2\sigma^2)$ .

161 To maintain a stable population, mortality increases with local population density. To do this we say  
 162 that individuals at distance  $d$  have a competitive interaction with strength  $g(d)$ , where  $g$  is the Gaussian  
 163 density with mean zero and standard deviation  $\sigma$ . Then, the sum of all competitive interactions with  
 164 individual  $i$  is  $n_i = \sum_j g(d_{ij})$ , where  $d_{ij}$  is the distance between individuals  $i$  and  $j$  and the sum is over  
 165 all neighbors within distance  $3\sigma$ . Since  $g$  is a probability density,  $n_i$  is an estimate of the number of  
 166 nearby individuals per unit area. Then, given a per-unit carrying capacity  $K$ , the probability of survival  
 167 until the next time step for individual  $i$  is

$$p_i = \min \left( 0.95, \frac{1}{1 + n_i / (K(1 + L))} \right). \quad (1)$$

168 We chose this functional form so that the equilibrium population density per unit area is close to  $K$ ,  
 169 and the mean lifetime is around  $L$ ; for more description see the Appendix.

170 An important step in creating any spatial model is dealing with range edges. Because local popula-  
 171 tion density is used to model competition, edge or corner populations can be assigned artificially high  
 172 fitness values because they lack neighbors within their interaction radius but outside the bounds of the  
 173 simulation. We approximate a decline in habitat suitability near edges by decreasing the probability  
 174 of survival proportional to the square root of distance to edges in units of  $\sigma$ . The final probability of  
 175 survival for individual  $i$  is then

$$s_i = p_i \min(1, \sqrt{x_i/\sigma}) \min(1, \sqrt{y_i/\sigma}) \min(1, \sqrt{(W - x_i)/\sigma}) \min(1, \sqrt{(W - y_i)/\sigma}) \quad (2)$$

176 where  $x_i$  and  $y_i$  are the spatial coordinates of individual  $i$ , and  $W$  is the width (and height) of the  
 177 square habitat. This buffer roughly counteracts the increase in fitness individuals close to the edge  
 178 would otherwise have, though the effect is relatively subtle (Figure S2).

179 To isolate spatial effects from other components of the model such as overlapping generations,  
 180 increased variance in reproductive success, and density-dependent fitness, we also implemented  
 181 simulations identical to those above except that mates are selected uniformly at random from the  
 182 population, and offspring disperse to a uniform random location on the landscape. We refer to this  
 183 model as the “random mating” model, in contrast to the first, “spatial” model.

184 We stored the full genealogy and recombination history of final-generation individuals as tree  
 185 sequences (Kelleher *et al.* 2018), as implemented in SLiM (Haller *et al.* 2019). Scripts for figures and  
 186 analyses are available at <https://github.com/kern-lab/spaceness>.

187 We ran 400 simulations for the spatial and random-mating models on a square landscape of width

188  $W = 50$  with per-unit carrying capacity  $K = 5$  (census  $N \approx 10,000$ ), average lifetime  $L = 4$ , genome  
189 size  $10^8$  bp, recombination rate  $10^{-9}$  per bp per generation, and drawing  $\sigma$  values from a uniform  
190 distribution between 0.2 and 4. To speed up the simulations and limit memory overhead we used a  
191 mutation rate of 0 in SLiM and later applied mutations to the tree sequence with msprime's `mutate`  
192 function (Kelleher *et al.* 2016). Because msprime applies mutations proportionally to elapsed time,  
193 we divided the mutation rate of  $10^{-8}$  mutations per site per generation by the average generation  
194 time estimated for each value of  $\sigma$  (see 'Demographic Parameters' below) to convert the rate to units  
195 of mutations per site per unit time. We verify that this procedure produces the same site frequency  
196 spectrum as applying mutations directly in SLiM in Figure S3, in agreement with theory (Ralph *et al.*  
197 2019b). Simulations were run for 1.6 million timesteps (approximately  $30N$  generations).

198 We also compared our model's output to a commonly-used approximation of continuous space,  
199 the stepping-stone model, which we simulated with msprime (Kelleher *et al.* 2016). These results are  
200 discussed in detail in the Appendix, but in general we find that the demographic structure of a stepping-  
201 stone model can depend strongly on the chosen discretization, and some artifacts of discretization seem  
202 to become stronger in the limit of a fine grid. For many summary statistics, finer discretizations (we  
203 used a  $50 \times 50$  grid) produced similar results to the continuous model, but this was not true for others  
204 (e.g.,  $F_{IS}$  and Tajima's  $D$ ), which differed from the continuous model *more* at finer discretizations.

## 205 **Demographic Parameters**

206 Our demographic model includes parameters that control population density ( $K$ ), mean life span ( $L$ ),  
207 and dispersal distance ( $\sigma$ ). However, nonlinearity of local demographic stochasticity causes actual  
208 realized averages of these demographic quantities to deviate from the specified values in a way that  
209 depends on the neighborhood size. Therefore, to properly compare to theoretical expectations, we  
210 empirically calculated these demographic quantities in simulations. We recorded the census population  
211 size in all simulations, and used mean population density ( $\rho$ , census size divided by total area) to  
212 compute neighborhood size as  $N_W = 4\pi\rho\sigma^2$ . To estimate generation times, we stored ages of the  
213 parents of every new individual born across 200 timesteps, after a 100 generation burn-in, and took the  
214 mean. To estimate variance in offspring number, we tracked the lifetime total number of offspring for  
215 all individuals for 100 timesteps following a 100-timestep burn-in period, and calculated the variance  
216 in number of offspring across all individuals in timesteps 50-100. All calculations were performed with  
217 information recorded in the tree sequence, using pyslim (Ralph *et al.* 2019a).

## 218 **Sampling**

219 Our model records the genealogy and sequence variation of the complete population, but in real data,  
220 genotypes are only observed from a relatively small number of sampled individuals. We modeled three  
221 sampling strategies similar to common data collection methods in empirical genetic studies (Figure 1).  
222 "Random" sampling selects individuals at random from across the full landscape, "point" sampling  
223 selects individuals proportional to their distance from four equally spaced points on the landscape,  
224 and "midpoint" sampling selects individuals in proportion to their distance from the middle of the  
225 landscape. Downstream analyses were repeated across all sampling strategies.

## 226 **Summary Statistics**

227 We calculated the site frequency spectrum and a set of 18 summary statistics (Table S1) from 60 diploid  
228 individuals sampled from the final generation of each simulation using the python package scikit-  
229 allel (Miles and Harding 2017). Statistics included common single-population summaries including  
230 mean pairwise divergence ( $\pi$ ), inbreeding coefficient ( $F_{IS}$ ), and Tajima's  $D$ , as well as (motivated by  
231 Rousset (1997)'s results) the correlation coefficient between the logarithm of the spatial distance and  
232 the proportion of identical base pairs across pairs of individuals.

233 Following recent studies that showed strong signals for dispersal and demography in the distri-  
234 bution of shared haplotype block lengths (e.g., Ringbauer *et al.* 2017; Baharian *et al.* 2016), we also  
235 calculated various summaries of the distribution of pairwise identical-by-state (IBS) block lengths  
236 among sampled chromosomes, defined to be the set of distances between adjacent sites that differ

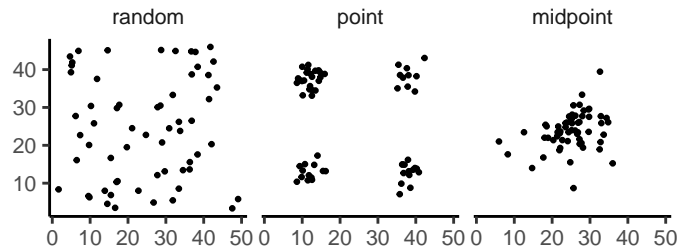


**Figure 1** Example sampling maps for 60 individuals on a  $50 \times 50$  landscape for midpoint, point, and random sampling strategies, respectively.

237 between the two chromosomes. The full distribution of lengths of IBS tracts for each pair of chromo-  
 238 somes was first calculated with a custom python function. We then calculated the first three moments  
 239 of this distribution (mean, variance, and skew) and the number of blocks over  $10^6$  base pairs both  
 240 for each pair of individuals and for the full distribution across all pairwise comparisons. We then  
 241 calculated correlation coefficients between spatial distance and each moment of the pairwise IBS tract  
 242 distribution. Because more closely related individuals on average share longer haplotype blocks we  
 243 expect that spatial distance will be negatively correlated with mean haplotype block length, and that  
 244 this correlation will be strongest (i.e., most negative) when dispersal is low. The variance, skew, and  
 245 count of long haplotype block statistics are meant to reflect the relative length of the right (upper) tail  
 246 of the distribution, which represents the frequency of long haplotype blocks, and so should reflect  
 247 recent demographic events (Chapman and Thompson 2002). For a subset of simulations, we also  
 248 calculated cumulative distributions for IBS tract lengths across pairs of distant (more than 40 map  
 249 units) and nearby (less than 10 map units) individuals. Last, we examined the relationship between  
 250 allele frequency and the spatial dispersion of an allele by calculating the average distance between  
 251 individuals carrying each derived allele.

252 The effects of sampling on summary statistic estimates were summarized by testing for differences  
 253 in mean (ANOVA, (R Core Team 2018)) and variance (Levene's test, (Fox and Weisberg 2011)) across  
 254 sampling strategies for each summary statistic.

#### 255 **Demographic Inference**

256 To assess the impacts of continuous spatial structure on demographic inference we inferred population  
 257 size histories for all simulations using two approaches: stairwayplot (Liu and Fu 2015) and SMC++  
 258 (Terhorst *et al.* 2016). Stairwayplot fits its model to a genome-wide estimate of the SFS, while SMC++  
 259 also incorporates linkage information. For both methods we sampled 20 individuals from all spatial  
 260 simulations using random, midpoint, and point sampling strategies.

261 As recommended by its documentation, we used stairwayplot to fit models with multiple bootstrap  
 262 replicates drawn from empirical genomic data, and took the median inferred  $N_e$  per unit time as  
 263 the best estimate. We calculated site frequency spectra with scikit-allel (Miles and Harding 2017),  
 264 generated 100 bootstrap replicates per simulation by resampling over sites, and fit models for all  
 265 bootstrap samples using default settings.

266 For SMC++, we first output genotypes as VCF with msprime and then used SMC++'s standard  
 267 pipeline for preparing input files assuming no polarization error in the SFS. We used the first individual  
 268 in the VCF as the "designated individual" when fitting models, and allowed the program to estimate  
 269 the recombination rate during optimization. We fit models using the 'estimate' command rather than  
 270 the now recommended cross-validation approach because our simulations had only a single contig.

271 To evaluate the performance of these methods we binned simulations by neighborhood size, took a  
 272 rolling median of inferred  $N_e$  trajectories across all model fits in a bin for each method and sampling  
 273 strategy. We also examined how varying levels of isolation by distance impacted the variance of  $N_e$   
 274 estimates by calculating the standard deviation of  $N_e$  from each best-fit model.

275 **Association Studies**

276 To assess the degree to which spatial structure confounds GWAS we simulated four types of nongenetic  
277 phenotype variation for 1000 randomly sampled individuals in each spatial SLiM simulation and  
278 conducted a linear regression GWAS with principal components as covariates in PLINK (Purcell *et al.*  
279 2007). SNPs with a minor allele frequency less than 0.5% were excluded from this analysis. Phenotype  
280 values were set to vary by two standard deviations across the landscape in a rough approximation  
281 of the variation seen in height across Europe (Turchin *et al.* 2012; Garcia and Quintana-Domeque  
282 2006, 2007). Conceptually our approach is similar to that taken by Mathieson and McVean (2012),  
283 though here we model fully continuous spatial variation and compare GWAS output across a range of  
284 dispersal distances.

285 In all simulations, the phenotype of each individual is determined by drawing from a Gaussian  
286 distribution with standard deviation 10 and a mean that may depend on spatial position. In spatially  
287 varying models, the mean phenotype differs by two standard deviations across the landscape. We  
288 then adjust the geographic pattern of mean phenotype to create four types of spatially autocorrelated  
289 environmental influences on phenotype. In the first simulation of *nonspatial* environments, the mean  
290 did not change, so that all individuals' phenotypes were drawn independently from a Gaussian  
291 distribution with mean 110 and standard deviation 10. Next, to simulate *clinal* environmental influences  
292 on phenotype, we increased the mean phenotype from 100 on the left edge of the range to 120 on the  
293 right edge (two phenotypic standard deviations). Concretely, the mean phenotype  $p$  for an individual  
294 at position  $(x, y)$  is  $p = 100 + 2x/5$ . Third, we simulated a more concentrated "*corner*" environmental  
295 effect by setting the mean phenotype to 120 for individuals with both  $x$  and  $y$  coordinates below 20  
296 (two standard deviations above the rest of the map). Finally, in "*patchy*" simulations we selected 10  
297 random points on the map and set the mean phenotype of all individuals within three map units of  
298 each of these points to 120.

299 We performed principal components analysis (PCA) using scikit-allel (Miles and Harding 2017) on  
300 the matrix of derived allele counts by individual for each simulation. SNPs were first filtered to remove  
301 strongly linked sites by calculating LD between all pairs of SNPs in a 200-SNP moving window and  
302 dropping one of each pair of sites with an  $R^2$  over 0.1. The LD-pruned allele count matrix was then  
303 centered and all sites scaled to unit variance when conducting the PCA, following recommendations  
304 in Patterson *et al.* (2006).

305 We ran linear-model GWAS both with and without the first 10 principal components as covariates  
306 in PLINK and summarized results across simulations by counting the number of SNPs with  $p$ -value  
307 below 0.05 after adjusting for an expected false positive rate of less than 5% (Benjamini and Yekutieli  
308 2001). We also examined  $p$  values for systematic inflation by comparing to the values expected from  
309 a uniform distribution (because no SNPs were used when generating phenotypes, well-calibrated  
310  $p$ -values should be uniform).

311 Results from all analyses were summarized and plotted with the "ggplot2" (Wickham 2016) and  
312 "cowplot" (Wilke 2019) packages in R (R Core Team 2018).

313 **Results**

314 **Demographic Parameters and Run Times**

315 Adjusting the spatial dispersal and interaction distance,  $\sigma$ , has a surprisingly large effect on de-  
316 mographic quantities that are usually fixed in Wright-Fisher models – the generation time, census  
317 population size, and variance in offspring number, shown in Figure 2. Because our simulation is  
318 parameterized on an individual level, these population parameters emerge as a property of the inter-  
319 actions among individuals rather than being directly set. Variation across runs occurs because, even  
320 though the parameters  $K$  and  $L$  that control population density and mean lifetime respectively were  
321 the same in all simulations, the strength of stochastic effects depends strongly on the spatial interaction  
322 distance  $\sigma$ . For instance, the population density near to individual  $i$  (denoted  $n_i$  above) is computed  
323 by averaging over roughly  $N_W = 4\pi K\sigma^2$  individuals, and so has standard deviation proportional to  
324  $1/\sqrt{N_W}$  – it is more variable at lower densities. (Recall that  $N_W$  is Wright's neighborhood size.) Since  
325 the probability of survival is a nonlinear function of  $n_i$ , actual equilibrium densities and lifetimes differ

326 from  $K$  and  $L$ . This is the reason that we included *random mating* simulations – where mate choice and  
 327 offspring dispersal are both nonspatial – since this should preserve the random fluctuations in local  
 328 population density while destroying any spatial genetic structure. We verified that random mating  
 329 models retained no geographic signal by showing that summary statistics did not differ significantly  
 330 between sampling regimes (Table S2), unlike in spatial models (discussed below).

331 There are a few additional things to note about Figure 2. First, all three quantities are non-monotone  
 332 with neighborhood size. Census size largely declines as neighborhood size increases for both the spatial  
 333 and random mating models. However, for spatial models this decline only begins for neighborhood  
 334 size  $\geq 10$ . Spatial and random mating models are indistinguishable from one another for neighborhood  
 335 sizes larger than 100. Census sizes range from around 14,000 at low  $\sigma$  in the random mating model  
 336 to 10,000 for both models when neighborhood sizes approach 1,000. The scaling of census sizes in  
 337 both random-mating and spatial models appears to be related to two consequences of the spatial  
 338 competition function: the decline of fitness at range edges, which effectively reduces the habitable area  
 339 by one  $\sigma$  around the edge of the map and so results in a smaller habitable area at high  $\sigma$  values; and  
 340 variation in the equilibrium population density given varying competition radii. Furthermore, census  
 341 size increases in spatial models as neighborhood size increases from 2 to 10. This may reflect an Allee  
 342 effect (Allee *et al.* 1949) in which some individuals are unable to find mates when the mate selection  
 343 radius is very small.

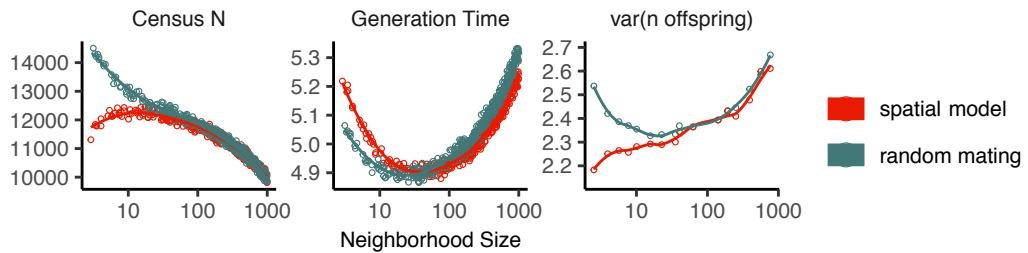


**Figure 2** Genealogical parameters from spatial and random mating SLiM simulations, by neighborhood size.

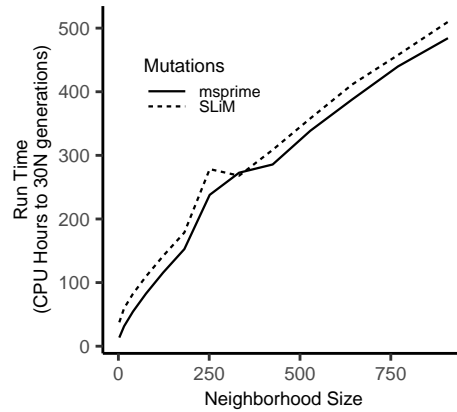


**Figure 3** Run times of continuous space simulations with landscape width 50 and expected density 5 under varying neighborhood size. Times are shown for simulations run with mutations applied directly in SLiM (dashed lines) or later applied to tree sequences with msprime (solid lines). Times for simulations run with tree sequence recording disabled are shown in grey.

344 Generation time similarly shows complex behavior with respect to neighborhood sizes, and varies

345 between 5.2 and 4.9 timesteps per generation across the parameter range explored. Under both the  
346 spatial and random mating models, generation time reaches a minimum at a neighborhood size of  
347 around 50. Interestingly, under the range of neighborhood sizes that we examined, generation times  
348 between the random mating and spatial models are never quite equivalent – presumably this would  
349 cease to be the case at neighborhood sizes higher than we simulated here.

350 Last, we looked at the variance in number of offspring – a key parameter determining the effective  
351 population size. Surprisingly, the spatial and random mating models behave quite differently: while  
352 the variance in offspring number increases nearly monotonically under the spatial model, the random  
353 mating model actually shows a decline in the variance in offspring number until a neighborhood size  
354 of around 10 before it increases and eventually equals what we observe in the spatial case.

355 Run times for our model scale approximately linearly with neighborhood size (Figure 3), with the  
356 lowest neighborhood sizes reaching 30N generations in around a day and those with neighborhood  
357 size approaching 1,000 requiring up to three weeks of computation. As currently implemented running  
358 simulations at neighborhood sizes more than 1,000 to coalescence is likely impractical, though running  
359 these models for more limited timescales and then “recapitulating” the simulation using reverse-time  
360 simulation from the resulting tree sequence in msprime is possible (Haller *et al.* 2019).

### 361 **Impacts of Continuous Space on Population Genetic Summary Statistics**

362 Even though certain aspects of population demography depend on the scale of spatial interactions, it  
363 still could be that population genetic variation is well-described by a well-mixed population model.  
364 Indeed, mathematical results suggest that genetic variation in some spatial models should be well-  
365 approximated by a Wright-Fisher population if neighborhood size is large and all samples are geo-  
366 graphically widely separated (Wilkins 2004; Zähle *et al.* 2005). However, the behavior of most common  
367 population genetic summary statistics other than Tajima’s *D* (Städler *et al.* 2009) has not yet been  
368 described in realistic geographic models. Moreover, as we will show, spatial sampling strategies can  
369 affect summaries of genetic variation at least as strongly as the underlying population dynamics.

370 **Site Frequency Spectra and Summaries of Diversity** Figure 4 shows the effect of varying neighbor-  
371 hood size and sampling strategy on the site frequency spectrum (Figure 4, Figure S5) and several  
372 standard population genetic summary statistics (Figure 4B; additional statistics are shown in Figure  
373 S4). Consistent with findings in island and stepping stone simulations (Städler *et al.* 2009), the SFS  
374 shows a significant enrichment of intermediate frequency variants in comparison to the nonspatial  
375 expectation. This bias is most pronounced below a neighborhood size of 100 and is exacerbated by  
376 midpoint and point sampling of individuals (depicted in Figure 1). Reflecting this, Tajima’s *D* is quite  
377 positive in the same situations (Figure 4B). Notably, the point at which Tajima’s *D* approaches 0 differs  
378 strongly across sampling strategies – varying from a neighborhood size of roughly 50 for random  
379 sampling to at least 1000 for midpoint sampling.

380 One of the most commonly used summaries of variation is Tajima’s summary of nucleotide diversity,  
381  $\theta_\pi$ , calculated as the mean density of nucleotide differences averaged across pairs of samples. As can  
382 be seen in Figure 4B,  $\theta_\pi$  in the spatial model is inflated by up to three-fold relative to the random  
383 mating model. This pattern is opposite the expectation from census population size (Figure 2), because  
384 the spatial model has *lower* census size than the random mating model at neighborhood sizes less than  
385 100. Differences between these models likely occur because  $\theta_\pi$  is a measure of mean time to most recent  
386 common ancestor between two samples, and at small values of  $\sigma$ , the time for dispersal to mix ancestry  
387 across the range exceeds the mean coalescent time under random mating. (For instance, at the smallest  
388 value of  $\sigma = 0.2$ , the range is 250 dispersal distances wide, and since the location of a diffusively  
389 moving lineage after  $k$  generations has variance  $k\sigma^2$ , it takes around  $250^2 = 62500$  generations to  
390 mix across the range, which is roughly ten times larger than the random mating effective population  
391 size).  $\theta_\pi$  using each sampling strategy approaches the random mating expectation at its own rate, but  
392 by a neighborhood size of around 100 all models are roughly equivalent. Interestingly, the effect of  
393 sampling strategy is reversed relative to that observed in Tajima’s *D* – midpoint sampling reaches  
394 random mating expectations around neighborhood size 50, while random sampling is inflated until  
395 around neighborhood size 100.



**Figure 4** Site frequency spectrum (A; note axes are log-scaled) and summary statistic distributions (B) by sampling strategy and neighborhood size.

396 Values of observed heterozygosity and its derivative  $F_{IS}$  also depend heavily on neighborhood size  
397 under spatial models as well as the sampling scheme.  $F_{IS}$  is inflated above the expectation across  
398 most of the parameter space examined and across all sampling strategies. This effect is caused by  
399 a deficit of heterozygous individuals in low-dispersal simulations – a continuous-space version of  
400 the Wahlund effect (Wahlund 1928). Indeed, for random sampling under the spatial model,  $F_{IS}$  does  
401 not approach the random mating equivalent until neighborhood sizes of nearly 1000. On the other  
402 hand, the dependency of raw observed heterozygosity on neighborhood size is not monotone. Under  
403 midpoint sampling observed heterozygosity is inflated even over the random mating expectation, as a  
404 result of the a higher proportion of heterozygotes occurring in the middle of the landscape (Figure S6).  
405 This echoes a report from Shirk and Cushman (2014) who observed a similar excess of heterozygosity  
406 in the middle of the landscape when simulating under a lattice model.

407 **IBS tracts and correlations with geographic distance** We next turn our attention to the effect of  
408 geographic distance on haplotype block length sharing, summarized for sets of nearby and distant  
409 individuals in Figure 5. There are two main patterns to note. First, nearby individuals share more  
410 long IBS tracts than distant individuals (as expected because they are on average more closely related).  
411 Second, the difference in the number of long IBS tracts between nearby and distant individuals  
412 decreases as neighborhood size increases. This reflects the faster spatial mixing of populations with  
413 higher dispersal, which breaks down the correlation between the IBS tract length distribution and  
414 geographic distance. This can also be seen in the bottom row of Figure 4B, where the correlation  
415 coefficients between the summaries of the IBS tract length distribution (the mean, skew, and count of  
416 tracts over  $10^6$ bp) and geographic distance approaches 0 as neighborhood size increases.

417 The patterns observed for correlations of IBS tract lengths with geographic distance are similar  
418 to those observed in the more familiar correlation of allele frequency measures such as  $D_{xy}$  (i.e.,  
419 “genetic distance”) or  $F_{ST}$  against geographic distance (Rousset 1997).  $D_{xy}$  is positively correlated  
420 with the geographic distance between the individuals, and the strength of this correlation declines  
421 as dispersal increases (Figure 4B), as expected (Wright 1943; Rousset 1997). This relationship is very  
422 similar across random and point sampling strategies, but is weaker for midpoint sampling, perhaps  
423 due to a dearth of long-distance comparisons. In much of empirical population genetics a regression  
424 of genetic differentiation against spatial distance is a de-facto metric of the significance of isolation  
425 by distance. The similar behavior of moments of the pairwise distribution of IBS tract lengths shows  
426 why haplotype block sharing has recently emerged as a promising source of information on spatial  
427 demography through methods described in Ringbauer *et al.* (2017) and Baharian *et al.* (2016).

428 **Spatial distribution of allele copies** Mutations occur in individuals and spread geographically over  
429 time. Because low frequency alleles generally represent recent mutations (Sawyer 1977; Griffiths *et al.*  
430 1999), the geographic spread of an allele may covary along with its frequency in the population. To  
431 visualize this relationship we calculated the average distance among individuals carrying a focal  
432 derived allele across simulations with varying neighborhood sizes, shown in Figure 6. On average  
433 we find that low frequency alleles are the most geographically restricted, and that the extent to which  
434 geography and allele frequency are related depends on the amount of dispersal in the population.  
435 For populations with large neighborhood sizes we found that even very low frequency alleles can be  
436 found across the full landscape, whereas in populations with low neighborhood sizes the relationship  
437 between distance among allele copies and their frequency is quite strong. This is the basic process  
438 underlying Novembre and Slatkin’s (2009) method for estimating dispersal distances based on the  
439 distribution of low frequency alleles, and also generates the greater degree of bias in GWAS effect sizes  
440 for low frequency alleles identified in Mathieson and McVean (2012).

#### 441 **Effects of Space on Demographic Inference**

442 One of the most important uses for population genetic data is inferring demographic history of popu-  
443 lations. As demonstrated above, the site frequency spectrum and the distribution of IBS tracts varies  
444 across neighborhood sizes and sampling strategies. Does this variation lead to different inferences of  
445 past population sizes? To ask this we inferred population size histories from samples drawn from our

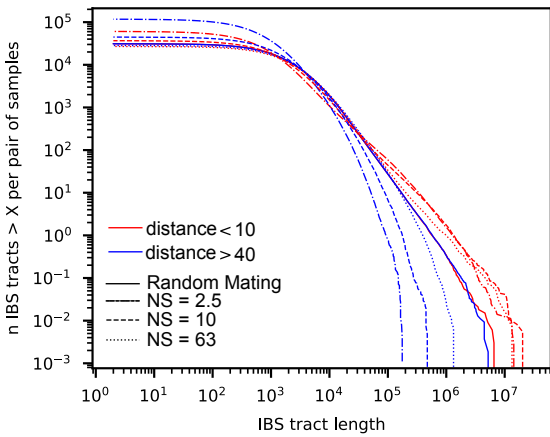


**Figure 5** Cumulative distributions for IBS tract lengths per pair of individuals at different geographic distances, across three neighborhood sizes (NS). Nearby pairs (red curves) share many more long IBS tracts than do distant pairs (blue curves), except in the random mating model. The distribution of long IBS tracts between nearby individuals are very similar across neighborhood sizes, but distant individuals are much more likely to share long IBS tracts at high neighborhood size than at low neighborhood size.

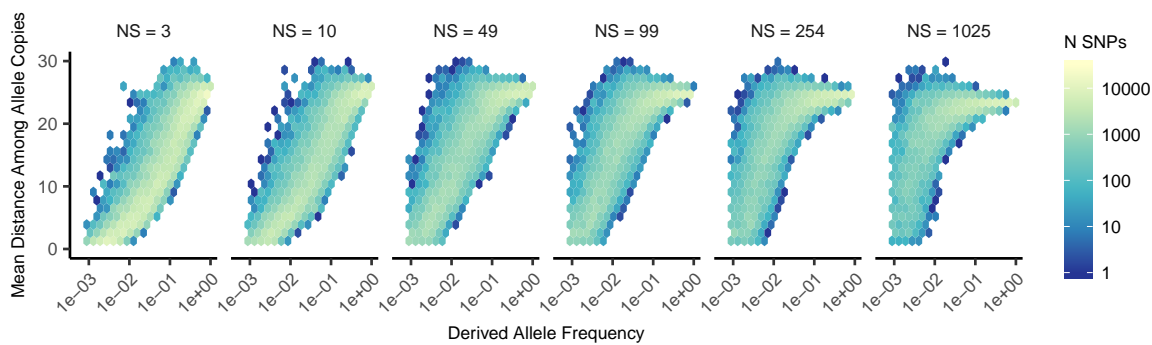


**Figure 6** Spatial spread of rare alleles by neighborhood size (NS): Each plot shows the distribution (across derived alleles and simulations) of average pairwise distance between individuals carrying a focal derived allele and derived allele frequency.

446 simulated populations with two approaches: stairwayplot (Liu and Fu 2015), which uses a genome-  
447 wide estimate of the SFS, and SMC++ (Terhorst *et al.* 2016), which incorporates information on both the  
448 SFS and linkage disequilibrium across the genome.

449 Figure 7A shows rolling medians of inferred population size histories from each method across all  
450 simulations, grouped by neighborhood size and sampling strategy. In general these methods tend to  
451 slightly overestimate ancient population sizes and infer recent population declines when neighborhood  
452 sizes are below 20 and sampling is spatially clustered. The overestimation of ancient population sizes  
453 however is relatively minor, averaging around a two-fold inflation at 10,000 generations before present  
454 in the worst-affected bins. For stairwayplot we found that many runs infer dramatic population  
455 bottlenecks in the last 1,000 generations when sampling is spatially concentrated, resulting in ten-fold  
456 or greater underestimates of recent population sizes. However SMC++ appeared more robust to  
457 this error, with runs on point- and midpoint-sampled simulations at the lowest neighborhood sizes  
458 underestimating recent population sizes by roughly half and those on randomly sampled simulations  
459 showing little error. Above neighborhood sizes of around 100, both methods performed relatively well  
460 when averaging across results from multiple simulations.

461 However, individual simulations were often inferred to have turbulent demographic histories, as  
462 shown by the individually inferred histories (shown in Figure S7). Indeed, the standard deviation of  
463 inferred  $N_e$  across time points (shown in Figure 7B) often exceeds the expected  $N_e$  for both methods.  
464 That is, despite the nearly constant population sizes in our simulations, both methods tended to infer  
465 large fluctuations in population size over time, which could potentially result in incorrect biological  
466 interpretations. On average the variance of inferred population sizes was elevated at the lowest  
467 neighborhood sizes and declines as dispersal increases, with the strongest effects seen in stairwayplot  
468 results with clustered sampling and neighborhood sizes less than 20 (Figure 7B).

#### 469 **GWAS**

470 To ask what confounding effects spatial genetic variation might have on genome-wide association  
471 studies we performed GWAS on our simulations using phenotypes that were determined solely by  
472 the environment – so, any SNP showing statistically significant correlation with phenotype is a false  
473 positive. As expected, spatial autocorrelation in the environment causes spurious associations across  
474 much of the genome if no correction for genetic relatedness among samples is performed (Figures 8 and  
475 S8). This effect is particularly strong for clinal and corner environments, for which the lowest dispersal  
476 levels cause over 60% of SNPs in the sample to return significant associations. Patchy environmental  
477 distributions, which are less strongly spatially correlated (Figure 8A), cause fewer false positives  
478 overall but still produce spurious associations at roughly 10% of sites at the lowest neighborhood  
479 sizes. Interestingly we also observed a small number of false positives in roughly 3% of analyses  
480 on simulations with nonspatial environments, both with and without PC covariates included in the  
481 regression.

482 The confounding effects of geographic structure are well known, and it is common practice to  
483 control for this by including principal components (PCs) as covariates to control for these effects. This  
484 mostly works in our simulations – after incorporating the first ten PC axes as covariates, the vast  
485 majority of SNPs no longer surpass a significance threshold chosen to have a 5% false discovery rate  
486 (FDR). However, a substantial number of SNPs – up to 1.5% at the lowest dispersal distances – still  
487 surpass this threshold (and thus would be false positives in a GWAS), especially under “corner” and  
488 “patchy” environmental distributions (Figure 8C). At neighborhood sizes larger than 500, up to 0.31%  
489 of SNPs were significant for corner and clinal environments. Given an average of 132,000 SNPs across  
490 simulations after MAF filtering, this translates to up to 382 false-positive associations; for human-sized  
491 genomes, this number would be much larger. In most cases the  $p$  values for these associations were  
492 significant after FDR correction but would not pass the threshold for significance under the more  
493 conservative Bonferroni correction (see example Manhattan plots in figure S8).

494 Clinal environments cause an interesting pattern in false positives after PC correction: at low  
495 neighborhood sizes the correction removes nearly all significant associations, but at neighborhood  
496 sizes above roughly 250 the proportion of significant SNPs increases to up to 0.4% (Figure 8). This may  
497 be due to a loss of descriptive power of the PCs – as neighborhood size increases, the total proportion of

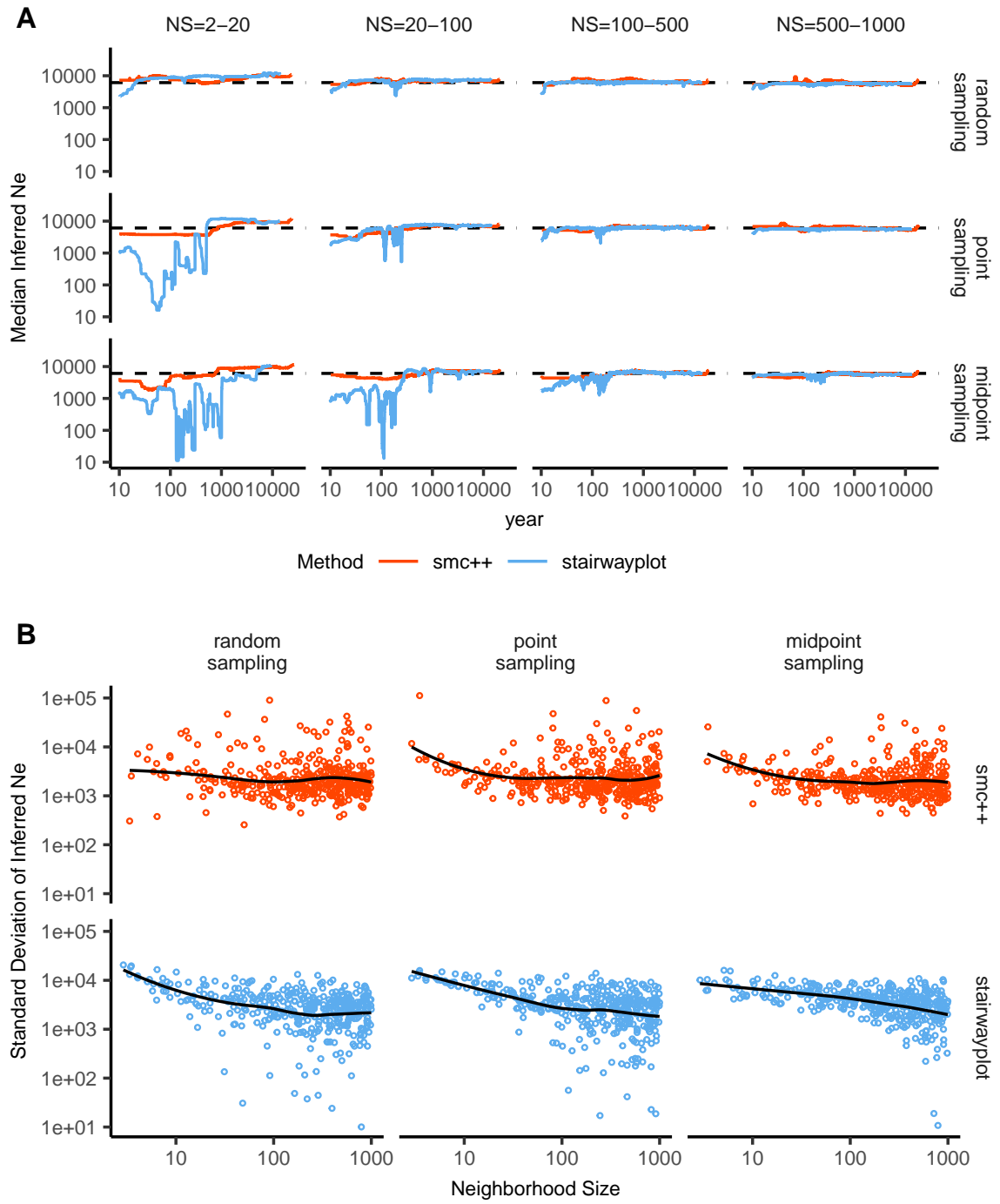


**Figure 7** A: Rolling median inferred  $N_e$  trajectories for stairwayplot and smc++ across sampling strategies and neighborhood size bins. The dotted line shows the mean  $N_e$  of random-mating simulations. B: Standard deviation of individual inferred  $N_e$  trajectories, by neighborhood size and sampling strategy. Black lines are loess curves. Plots including individual model fits are shown in Figure S7.

498 variance explained by the first 10 PC axes declines from roughly 10% to 4% (Figure 8B). Essentially, PCA  
499 seems unable to effectively summarize the weak population structure present in large-neighborhood  
500 simulations given the sample sizes we tested, but these populations continue to have enough spatial  
501 structure to create significant correlations between genotypes and the environment. A similar process  
502 can also be seen in the corner phenotype distribution, in which the count of significant SNPs initially  
503 declines as neighborhood size increases and then increases at approximately the point at which the  
504 proportion of variance explained by PCA approaches its minimum.

505 Figure 8D shows quantile-quantile plots for a subset of simulations that show the degree of genome-  
506 wide inflation of test statistics in PC-corrected GWAS across all simulations and environmental distri-  
507 butions. An alternate visualization is also included in figure S9. For clinal environments,  $-\log_{10}(p)$   
508 values are most inflated when neighborhood sizes are large, consistent with the pattern observed in  
509 the count of significant associations after PC regression. In contrast corner and patchy environments  
510 cause the greatest inflation in  $-\log_{10}(p)$  at neighborhood sizes less than 100, which likely reflects  
511 the inability of PCA to account for fine-scale structure caused by very limited dispersal. Finally, we  
512 observed that PC regression appears to overfit to some degree for all phenotype distributions, visible  
513 in Figure 8D as points falling below the 1:1 line.

## 514 Discussion

515 In this study, we have used efficient forward time population genetic simulations to describe the  
516 myriad influence of continuous geography on genetic variation. In particular, we examine how three  
517 main types of downstream empirical inference are affected by unmodeled spatial population structure  
518 – population genetic summary statistics, inference of population size history, and genome-wide associ-  
519 ation studies (GWAS). As discussed above, space often matters (and sometimes dramatically), both  
520 because of how samples are arranged in space, and because of the inherent patterns of relatedness  
521 established by geography.

### 522 Effects of Dispersal

523 Limited dispersal inflates effective population size, creates correlations between genetic and spatial  
524 distances, and introduces strong distortions in the site frequency spectrum that are reflected in a  
525 positive Tajima's  $D$  (Figure 4). At the lowest dispersal distances, this can increase genetic diversity  
526 threefold relative to random-mating expectations. These effects are strongest when neighborhood  
527 sizes are below 100, but in combination with the effects of nonrandom sampling they can persist up to  
528 neighborhood sizes of at least 1000 (e.g., inflation in Tajima's  $D$  and observed heterozygosity under  
529 midpoint sampling). If samples are chosen uniformly from across space, the general pattern is similar  
530 to expectations of the original analytic model of Wright (1943), which predicts that populations with  
531 neighborhood sizes under 100 will differ substantially from random mating, while those above 10,000  
532 will be nearly indistinguishable from panmixia.

533 The patterns observed in sequence data reflect the effects of space on the underlying genealogy.  
534 Nearby individuals coalesce rapidly under limited dispersal and so are connected by short branch  
535 lengths, while distant individuals take much longer to coalesce than they would under random  
536 mating. Mutation and recombination events in our simulation both occur at a constant rate along  
537 branches of the genealogy, so the genetic distance and number of recombination events separating  
538 sampled individuals simply gives a noisy picture of the genealogies connecting them. Tip branches  
539 (i.e., branches subtending only one individual) are then relatively short, and branches in the middle of  
540 the genealogy connecting local groups of individuals relatively long, leading to the biases in the site  
541 frequency spectrum shown in Figure 4.

542 The genealogical patterns introduced by limited dispersal are particularly apparent in the distribu-  
543 tion of haplotype block lengths (Figure 4). This is because identical-by-state tract lengths reflect the  
544 impacts of two processes acting along the branches of the underlying genealogy – both mutation and  
545 recombination – rather than just mutation as is the case when looking at the site frequency spectrum or  
546 related summaries. This means that the pairwise distribution of haplotype block lengths carries with  
547 it important information about genealogical variation in the population, and correlation coefficients

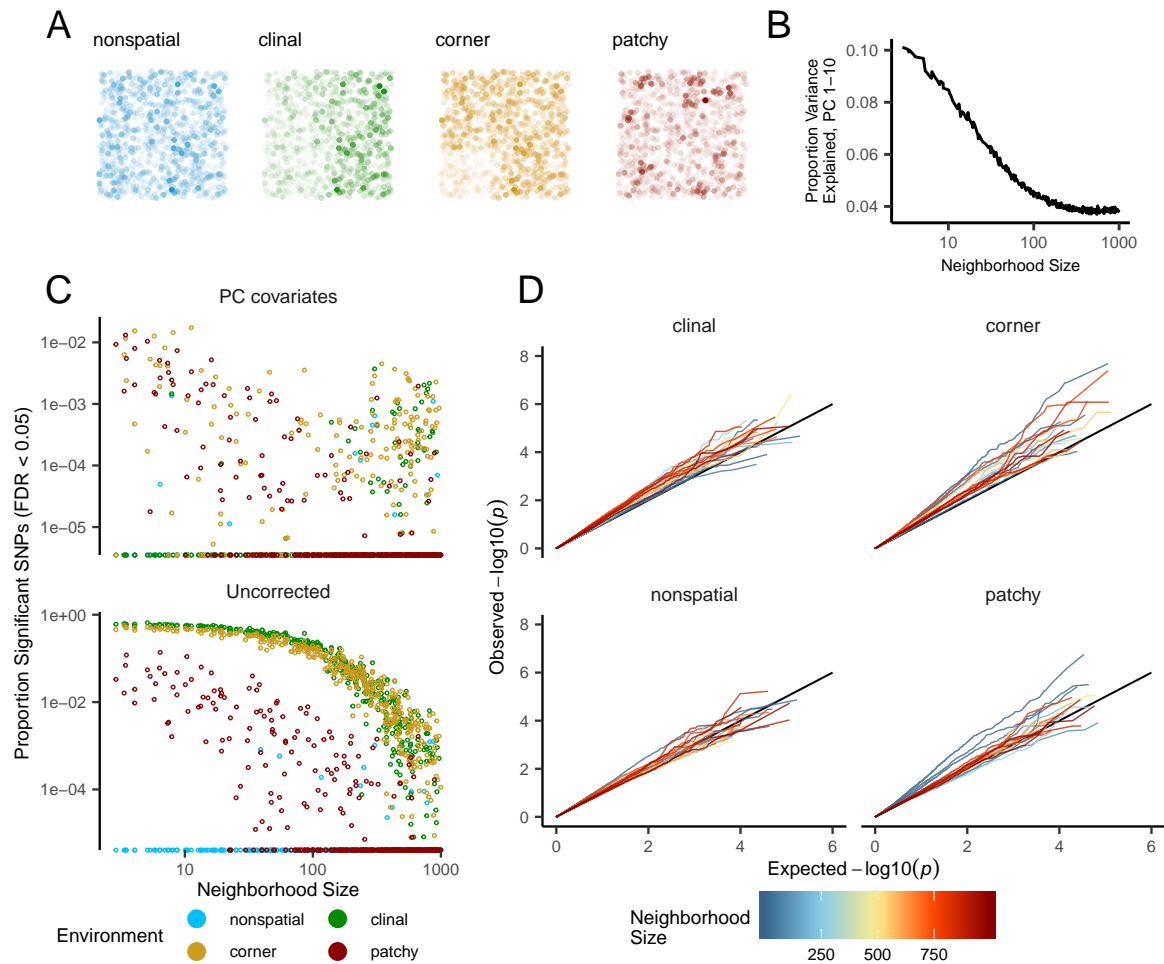


**Figure 8** Impacts of spatially varying environments and isolation by distance on linear regression GWAS. Simulated quantitative phenotypes are determined only by an individual's location and the spatial distribution of environmental factors. In **A** we show the phenotypes and locations of sampled individuals under four environmental distributions, with transparency scaled to phenotype. As neighborhood size increases a PCA explains less of the total variation in the data (**B**). Spatially correlated environmental factors cause false positives at a large proportion of SNPs, which is partially but not entirely corrected by adding the first 10 PC coordinates as covariates (**C**). Quantile-quantile plots in **(D)** show inflation of  $-\log_{10}(p)$  after PC correction for simulations with spatially structured environments, with line colors showing the neighborhood size of each simulation.

548 between moments of the this distribution and geographic location contain signal similar to the correlations  
549 between  $F_{ST}$  or  $D_{xy}$  and geographic distance (Rousset 1997). Indeed this basic logic underlies  
550 two recent studies explicitly estimating dispersal from the distribution of shared haplotype block  
551 lengths (Ringbauer *et al.* 2017; Baharian *et al.* 2016). Conversely, because haplotype-based measures of  
552 demography are particularly sensitive to variation in the underlying genealogy, inference approaches  
553 that assume random mating when analyzing the distribution of shared haplotype block lengths are  
554 likely to be strongly affected by spatial processes.

### 555 **Effects of Sampling**

556 One of the most important differences between random mating and spatial models is the effect of  
557 sampling: in a randomly mating population the spatial distribution of sampling effort has no effect on  
558 estimates of genetic variation (Table S1), but when dispersal is limited sampling strategy can compound  
559 spatial patterns in the underlying genealogy and create pervasive impacts on all downstream genetic  
560 analyses (see also Städler *et al.* (2009)). In most species, the difficulty of traveling through all parts  
561 of a species range and the inefficiency of collecting single individuals at each sampling site means  
562 that most studies follow something closest to the “point” sampling strategy we simulated, in which  
563 multiple individuals are sampled from nearby points on the landscape. For example, in ornithology a  
564 sample of 10 individuals per species per locality is a common target when collecting for natural history  
565 museums. In classical studies of *Drosophila* variation the situation is considerably worse, in which a  
566 single orchard might be extensively sampled.

567 When sampling is clustered at points on a landscape and dispersal is limited, the sampled individ-  
568 uals will be more closely related than a random set of individuals. Average coalescence times of  
569 individuals collected at a locality will then be more recent and branch lengths shorter than expected by  
570 analyses assuming random mating. This leads to fewer mutations and recombination events occurring  
571 since their last common ancestor, causing a random set of individuals to share longer average IBS tracts  
572 and have fewer nucleotide differences. For some data summaries, such as Tajima’s  $D$ , Watterson’s  
573  $\theta$ , or the correlation coefficient between spatial distance and the count of long haplotype blocks, this  
574 can result in large differences in estimates between random and point sampling (Figure 4). Inferring  
575 underlying demographic parameters from these summary statistics – unless the spatial locations of the  
576 sampled individuals are somehow taken into account – will likely be subject to bias.

577 We observed the largest sampling effects using “midpoint” sampling. This model is meant to  
578 reflect a bias in sampling effort towards the middle of a species’ range. In empirical studies this  
579 sampling strategy could arise if, for example, researchers choose to sample the center of the range  
580 and avoid range edges to maximize probability of locating individuals during a short field season.  
581 Because midpoint sampling provides limited spatial resolution it dramatically reduces the magnitude  
582 of observed correlations between spatial and genetic distances. More surprisingly, midpoint sampling  
583 also leads to strongly positive Tajima’s  $D$  and an inflation in the proportion of heterozygous individuals  
584 in the sample – similar to the effect of sampling a single deme in an island model as reported in Städler  
585 *et al.* (2009). This increase in observed heterozygosity appears to reflect the effects of range edges,  
586 which are a fundamental facet of spatial genetic variation. If individuals move randomly in a finite  
587 two-dimensional landscape then regions in the middle of the landscape receive migrants from all  
588 directions while those on the edge receive no migrants from at least one direction. The average number  
589 of new mutations moving into the middle of the landscape is then higher than the number moving  
590 into regions near the range edge, leading to higher heterozygosity and lower inbreeding coefficients  
591 ( $F_{IS}$ ) away from range edges. Though here we used only a single parameterization of fitness decline at  
592 range edges we believe this is a general property of non-infinite landscapes as it has also been observed  
593 in previous studies simulating under lattice models (Neel *et al.* 2013; Shirk and Cushman 2014).

594 In summary, we recommend that empirical researchers collect individuals from across as much  
595 of the species’ range as practical, choosing samples separated by a range of spatial scales. Many  
596 summary statistics are designed for well-mixed populations, and so provide different insights into  
597 genetic variation when applied to different subsets of the population. Applied to a cluster of samples,  
598 summary statistics based on segregating sites (e.g., Watterson’s  $\theta$  and Tajima’s  $D$ ), heterozygosity, or  
599 the distribution of long haplotype blocks, can be expected to depart significantly from what would be

600 obtained from a wider distribution of samples. Comparing the results of analyses conducted on all  
601 individuals versus those limited to single individuals per locality can provide an informative contrast.  
602 Finally we wish to point out that the bias towards intermediate allele frequencies that we observe may  
603 mean that the importance of linked selection, at least as is gleaned from the site frequency spectrum,  
604 may be systematically underestimated currently.

605 **Demography**

606 Previous studies have found that population structure and nonrandom sampling can create spurious  
607 signals of population bottlenecks when attempting to infer demographic history with microsatellite  
608 variation, summary statistics, or runs of homozygosity (Chikhi *et al.* 2010; Städler *et al.* 2009; Ptak  
609 and Przeworski 2002; Mazet *et al.* 2015; Leblois *et al.* 2006). Here we found that methods that infer  
610 detailed population trajectories through time based on the SFS and patterns of LD across the genome  
611 are also subject to this bias, with some combinations of dispersal and sampling strategy systematically  
612 inferring deep recent population bottlenecks and overestimating ancient  $N_e$  by around a factor of 2.  
613 We were surprised to see that both stairwayplot and SMC++ can tolerate relatively strong isolation by  
614 distance – i.e., neighborhood sizes of 20 – and still perform well when averaging results across multiple  
615 simulations. Inference in populations with neighborhood sizes over 20 was relatively unbiased unless  
616 samples were concentrated in the middle of the range (Figure 7). Although median demography  
617 estimates across many independent simulations were fairly accurate, empirical work has only a  
618 single estimate to work with, and individual model fits (Figure S7) suggest that spuriously inferred  
619 population size changes and bottlenecks are common, especially at small neighborhood sizes. As we  
620 will discuss below, most empirical estimates of neighborhood size, including all estimates for human  
621 populations, are large enough that population size trajectories inferred by these approaches should not  
622 be strongly affected by spatial biases created by dispersal in continuous landscapes. In contrast, Mazet  
623 *et al.* (2015) found that varying migration rates through time could create strong biases in inferred  
624 population trajectories from an  $n$ -island model with parameters relevant for human history, suggesting  
625 that changes in migration rates through time are more likely to drive variation in inferred  $N_e$  than  
626 isolation by distance.

627 We found that SMC++ was more robust to the effects of space than stairwayplot, underestimating  
628 recent populations by roughly half in the worst time periods rather than nearly 10-fold as with  
629 stairwayplot. Though this degree of variation in population size is certainly meaningful in an ecological  
630 context, it is relatively minor in population genetic terms. Methods directly assessing haplotype  
631 structure in phased data example, (e.g., Browning and Browning 2015) are thought to provide increased  
632 resolution for recent demographic events, but in this case the error we observed was essentially an  
633 accurate reflection of underlying genealogies in which terminal branches are anomalously short.  
634 Combined with our analysis of IBS tract length variation (Figure 5) this suggests that haplotype-based  
635 methods are likely to be affected by similar biases.

636 A more worrying pattern was the high level of variance in inferred  $N_e$  trajectories for individual  
637 model fits using these methods, which was highest in simulations with the smallest neighborhood  
638 size (Figure 7, Figure S7). This suggests that, at a minimum, researchers working with empirical data  
639 should replicate analyses multiple times and take a rolling average if model fits are inconsistent across  
640 runs. Splitting samples and running replicates on separate subsets – the closest an empirical study can  
641 come to our design of averaging the results from multiple simulations – may also alleviate this issue.

642 Our analysis suggests that many empirical analyses of population size history using methods like  
643 SMC++ are robust to error caused by spatial structure within continuous landscapes. Inferences drawn  
644 from static SFS-based methods like stairwayplot should be treated with caution when there are signs  
645 of isolation by distance in the underlying data (for example, if a regression of  $F_{ST}$  against the logarithm  
646 of geographic distance has a significantly positive slope), and in particular an inference of population  
647 bottlenecks in the last 1000 years should be discounted if sampling is clustered, but estimates of deeper  
648 time patterns are likely to be fairly accurate. The biases in the SFS and haplotype structure identified  
649 above (see also Wakeley 1999; Chikhi *et al.* 2010; Städler *et al.* 2009) are apparently small enough that  
650 they fall within the range of variability regularly inferred by these approaches, at least on datasets of  
651 the size we simulated.

652 **GWAS**

653 Spatial structure is particularly challenging for genome-wide association studies, because the effects of  
654 dispersal on genetic variation are compounded by spatial variation in the environment (Mathieson  
655 and McVean 2012). Spatially restricted mate choice and dispersal causes variation in allele frequencies  
656 across the range of a species. If environmental factors affecting the phenotype of interest also vary over  
657 space, then allele frequencies and environmental exposures will covary over space. In this scenario an  
658 uncorrected GWAS will infer genetic associations with a purely environmental phenotype at any site  
659 in the genome that is differentiated over space, and the relative degree of bias will be a function of the  
660 degree of covariation in allele frequencies and the environment (i.e., Figure 8C, bottom panel). This  
661 pattern has been demonstrated in a variety of simulation and empirical contexts (Price *et al.* 2006; Yu  
662 *et al.* 2005; Young *et al.* 2018; Mathieson and McVean 2012; Kang *et al.* 2008, 2010; Bulik-Sullivan *et al.*  
663 2015; Berg *et al.* 2018; Sohail *et al.* 2018).

664 Incorporating PC positions as covariates in a linear-regression GWAS (Price *et al.* 2006) is designed  
665 to address this challenge by regressing out a baseline level of “average” differentiation. In essence, a  
666 PC-corrected GWAS asks “what regions of the genome are more associated with this phenotype than  
667 the average genome-wide association observed across populations?” In our simulations, we observed  
668 that this procedure can fail under a variety of circumstances. If dispersal is limited and environmental  
669 variation is clustered in space (i.e., corner or patchy distributions in our simulations), PC positions fail  
670 to capture the fine-scale spatial structure required to remove all signals of association. Conversely, as  
671 dispersal increases, PCA loses power to describe population structure before spatial mixing breaks  
672 down the relationship between genotype and the environment. These effects were observed with all  
673 spatially correlated environmental patterns, but were particularly pronounced if environmental effects  
674 are concentrated in one region, as was also found by Mathieson and McVean (2012). Though increasing  
675 the number of PC axes used in the analysis may reduce the false-positive rate, this may also decrease  
676 the power of the test to detect truly causal alleles (Lawson *et al.* 2019).

677 In this work we simulated a single chromosome with size roughly comparable to one human  
678 chromosome. If we scale the number of false-positive associations identified in our analyses to a  
679 GWAS conducted on whole-genome data from humans, we would expect to see several thousand  
680 weak false-positive associations after PC corrections in a population with neighborhood sizes up to at  
681 least 1000 (which should include values appropriate for many human populations). Notably, very few  
682 of the spurious associations we identified would be significant at a conservative Bonferroni-adjusted  
683 *p*-value cutoff (see Figure S8). This suggests that GWAS focused on finding strongly associated alleles  
684 for traits controlled by a limited number of variants in the genome are likely robust to the impacts  
685 of continuous spatial structure. However, methods that analyze the combined effects of thousands  
686 or millions of weakly associated variants such as polygenic risk scores (Khera *et al.* 2018) are likely  
687 to be affected by subtle population structure. Indeed as recently identified in studies of genotype  
688 associations for human height in Europe (Berg *et al.* 2018; Sohail *et al.* 2018), PC regression GWAS in  
689 modern human populations do include residual signal of population structure in large-scale analyses  
690 of polygenic traits. In addition to error associated with varying patterns of linkage disequilibrium  
691 and allele frequency among populations, the confounding of environmental and genetic effects on  
692 phenotypes introduced by population structure is expected to lead to low predictive power when  
693 polygenic scores are generated for populations outside the original GWAS cohort, as was shown in a  
694 recent study finding lower polygenic score predictive power outside European populations (Martin  
695 *et al.* 2019).

696 In summary, spatial covariation in population structure and the environment confounds the interpretation  
697 of GWAS *p*-values, and correction using principal components is insufficient to fully separate these signals for polygenic traits under a variety of environmental and population parameter  
698 regimes. Other GWAS methods such as mixed models (Kang *et al.* 2008) may be less sensitive to this  
700 confounding, but there is no obvious reason that this should be so. One approach to estimating the degree of bias in GWAS caused by population structure is LD score regression (Bulik-Sullivan  
702 *et al.* 2015). Though this approach appears to work well in practice, its interpretation is not always  
703 straightforward and it is likely biased by the presence of linked selection (Berg *et al.* 2018). In addition,

704 we observed that in many cases the false-positive SNPs we identified appeared to be concentrated in  
 705 LD peaks similar to those expected from truly causal sites (Figure S8), which may confound LD score  
 706 regression.

707 We suggest a straightforward alternative for species in which the primary axes of population  
 708 differentiation is space (note this is likely not the case for some modern human populations): run a  
 709 GWAS with spatial coordinates as phenotypes and check for *p*-value inflation or significant associations.  
 710 If significant associations with sample locality are observed after correcting for population structure,  
 711 the method is sensitive to false positives induced by spatial structure. This is essentially the approach  
 712 taken in our “clinal” model (though we add normally distributed noise to our phenotypes). This  
 713 approach has recently been taken with polygenic scores for UK Biobank samples in Haworth *et al.*  
 714 (2019), finding that scores are correlated with birth location even in this relatively homogenous sample.  
 715 Of course, it is possible that genotypes indirectly affect individual locations by adjusting organismal  
 716 fitness and thus habitat selection across spatially varying environments, but we believe that this  
 717 hypothesis should be tested against a null of stratification bias inflation rather than accepted as true  
 718 based on GWAS results.

**Table 1 Neighborhood size estimates from empirical studies.**

Species	Description	Neighborhood Size	Method	Citation
<i>Ipomopsis aggregata</i>	flowering plant	12.60 - 37.80	Genetic	(Campbell and Dooley 1992)
<i>Borreria frutescens</i>	salt marsh plant	20 - 30	Genetic+Survey	(Antlfinger 1982)
<i>Oreamnos americanus</i>	mountain goat	36 - 100	Genetic	(Shirk and Cushman 2014)
<i>Homo sapiens</i>	Gainj- and Kalam-speaking people, Papua New Guinea	40 - 213	Genetic	(Rousset 1997)
<i>Formica sp.</i>	colonial ants	50 - 100	Genetic	(Pamilo 1983)
<i>Astrocaryum mexicanum</i>	palm tree	102 - 895	Genetic+survey	(Eguiarte <i>et al.</i> 1993)
<i>Spermophilus mollis</i>	ground squirrel	204 - 480	Genetic+Survey	(Antolin <i>et al.</i> 2001)
<i>Sceloporus olivaceus</i>	lizard	225 - 270	Survey	(Kerster 1964)
<i>Dieffenbachia longispatha</i>	beetle-pollinated colonial herb	227 - 611	Survey	(Young 1988)
<i>Aedes aegypti</i>	Yellow-fever mosquito	268	Genetic	(Jasper <i>et al.</i> 2019)
<i>Homo sapiens</i>	Gainj- and Kalam-speaking people, Papua New Guinea	410	Survey	(Rousset 1997)
<i>Quercus laevis</i>	Oak tree	> 440	Genetic	(Berg and Hamrick 1995)
<i>Drosophila pseudoobscura</i>	fruit fly	500 - 1,000	Survey+Crosses	(Wright 1946)
<i>Homo sapiens</i>	POPRES data NE Europe	1,342 - 5,425	Genetic	(Ringbauer <i>et al.</i> 2017)

719 **Where are natural populations on this spectrum?**

720 For how much of the tree of life do spatial patterns circumscribe genomic variation? In Table 1 we  
 721 gathered estimates of neighborhood size from a range of organisms to get an idea of how strongly local  
 722 geographic dispersal affects patterns of variation. This is an imperfect measure: some aspects of genetic

723 variation are most strongly determined by neighborhood size (Wright 1946), others (e.g., number of  
724 segregating sites) by global  $N_e$ , or the ratio of the two. In addition, definitions of "population density"  
725 in genetic versus ecological studies may lead to varying estimates of neighborhood size for a given  
726 species, and these empirical examples may be biased towards small-neighborhood species because few  
727 studies have quantified neighborhood size in species with very high dispersal or population density.

728 However, from the available data we find that neighborhood sizes in the range we simulated are  
729 fairly common across a range of taxa. At the extreme low end of empirical neighborhood size estimates  
730 we see some flowering plants, large mammals, and colonial insects like ants with neighborhood sizes  
731 less than roughly 100. Species such as this have neighborhood size estimates small enough that spatial  
732 processes are likely to strongly influence inference. These include some human populations such as  
733 the Gainj- and Kalam-speaking people of Papua New Guinea, in which the estimated neighborhood  
734 sizes in Rousset (1997) range from 40 to 410 depending on the method of estimation. Many more  
735 species occur in a middle range of neighborhood sizes between 100 and 1000 – a range in which spatial  
736 processes play a minor role in our analyses under random spatial sampling but are important when  
737 sampling of individuals in space is clustered. Surprisingly, even some flying insects with huge census  
738 population sizes fall in this group, including fruit flies (*D. melanogaster*) and mosquitoes (*A. aegypti*).  
739 Last, many species likely have neighborhood sizes much larger than we simulated, including the  
740 recent ancestors of modern humans in northeastern Europe (Ringbauer *et al.* 2017). For these species  
741 demographic inference and summary statistics are likely to reflect minimal bias from spatial effects as  
742 long as dispersal is truly continuous across the landscape. While that is so we caution that association  
743 studies in which the effects of population structure are confounded with spatial variation in the  
744 environment are still sensitive to dispersal even at these large neighborhood sizes.

#### 745 **Other demographic models**

746 Any simulation of a population of reproducing organisms requires some kind of control on population  
747 sizes, or else the population will either die out or grow very large after a sufficiently long period  
748 of time. The usual choice of population regulation for population genetics – a constant size, as  
749 in the Wright–Fisher model – implies biologically unrealistic interactions between geographically  
750 distant parts of the species range. Our choice to regulate population size by including a local density-  
751 dependent control on mortality is only one of many possible ways to do this. We could have instead  
752 regulated fecundity, or recruitment, or both; this general class of models is sometimes referred to as  
753 the “Bolker–Pacala model” (Bolker and Pacala 1997). It is not currently clear how much different  
754 choices of demographic parameters, or of functional forms for the regulation, might quantitatively  
755 affect our results, although the general predictions should be robust to similar forms of regulation.  
756 Since populations are still entirely *intrinsically* regulated, our model still has a very strong “population  
757 genetics” flavor. Alternatively, population size could be regulated by interactions with other species  
758 (e.g., a Lotka–Volterra model), or extrinsically specified by local resource availability (e.g., by food  
759 or nest site availability). Indeed, our model could be interpreted as a caricature of such a model: as  
760 local density increases, good habitat is increasingly occupied, pushing individuals into more marginal  
761 habitat and increasing their mortality. Many such models should behave similarly to ours, but others  
762 (especially those with local population cycling), may differ dramatically.

763 Population genetic simulations often use grids of discrete demes, which are assumed to approximate  
764 continuous space. However, there are theoretical reasons to expect that increasingly fine grids of  
765 discrete demes do not approach the continuous model (Barton *et al.* 2002). If continuous space can  
766 be approximated by a limit of discrete models, this should be true regardless of the precise details  
767 of the discrete model. Although we carefully chose parameters to match our continuous models, we  
768 found that some aspects of genetic variation diverged from the continuous case as the discretization  
769 got finer. This suggests that these models do not converge in the limit. However, many populations  
770 may indeed be well-modeled as a series of discrete, randomly-mating demes if, for example, suitable  
771 habitats are patchily distributed across the landscape. There is a clear need for greater exploration of  
772 the consequences for population genetics of ecologically realistic population models.

773 **Future Directions and Limitations**

774 As we have shown, a large number of population genetic summary statistics contain information about  
775 spatial population processes. We imagine that combinations of such summaries might be sufficient  
776 for the construction of supervised machine learning regressors (e.g., Schrider and Kern 2018) for the  
777 accurate estimation of dispersal from genetic data. Indeed, Ashander *et al.* (2018) found that inverse  
778 interpolation on a vector of summary statistics provided a powerful method of estimating dispersal  
779 distances. Expanding this approach to include the haplotype-based summary statistics studied here  
780 and applying machine learning regressors built for general inference of nonlinear relationships from  
781 high-dimensional data may allow precise estimation of spatial parameters under a range of complex  
782 models.

783 One facet of spatial variation that we did not address in this study is the confounding of dispersal  
784 and population density implicit in the definition of Wright's neighborhood size. Our simulations were  
785 run under constant densities, but Guindon *et al.* (2016) and Ringbauer *et al.* (2017) have shown that  
786 these parameters are identifiable under some continuous models. Similarly, though the scaling effects  
787 of dispersal we show in Figure 4 should occur in populations of any total size, other aspects such as the  
788 number of segregating sites are also likely affected by the total landscape size (and so total census size).  
789 Indeed, our finding that stepping-stone models reproduce only some of the effects on genetic variation  
790 seen in a continuous-space model (Figure A1) suggests that qualitatively similar models can produce  
791 different results dependent on the specific parameterizations used. While we believe our continuous  
792 model is a more appropriate depiction of evolution in a continuous landscape than lattice models, it is  
793 likely that some populations and breeding systems do more closely resemble a series of interconnected  
794 random-mating populations. As with all population models, the best approximation for any empirical  
795 system will depend on the natural history of the species in question. Much additional work remains  
796 to be done to better understand how life history and range size interact to shape genetic variation in  
797 continuous space, which we leave to future studies.

798 Though our simulation allows incorporation of realistic demographic and spatial processes, it  
799 is inevitably limited by the computational burden of tracking tens or hundreds of thousands of  
800 individuals in every generation. In particular, computations required for mate selection and spatial  
801 competition scale approximately with the product of the total census size and the neighborhood  
802 size and so increase rapidly for large populations and dispersal distances. The reverse-time spatial  
803 Lambda–Fleming–Viot model described by Barton *et al.* (2010) and implemented by Kelleher *et al.*  
804 (2014) allows exploration of larger population and landscape sizes, but the precise connection of these  
805 models to forward-time demography is not yet clear. Alternatively, implementation of parallelized  
806 calculations may allow progress with forward-time simulations.

807 Finally, we believe that the difficulties in correcting for population structure in continuous populations  
808 using principal components analysis or similar decompositions is a difficult issue, well worth  
809 considering on its own. How can we best avoid spurious correlations while correlating genetic and  
810 phenotypic variation without underpowering the methods? Perhaps optimistically, we posit that  
811 process-driven descriptions of ancestry and/or more generalized unsupervised methods may be able  
812 to better account for carry out this task.

813 **Data Availability**

814 Scripts used for all analyses and figures are available at <https://github.com/kern-lab/spaceness>.

815 **Acknowledgements**

816 We thank Brandon Cooper, Matt Hahn, Doc Edge, and others for reading and thinking about this  
817 manuscript. CJB and ADK were supported by NIH award R01GM117241.

818 **Literature Cited**

819 Aguillon, S. M., J. W. Fitzpatrick, R. Bowman, S. J. Schoech, A. G. Clark, *et al.*, 2017 Deconstructing  
820 isolation-by-distance: The genomic consequences of limited dispersal. PLOS Genetics 13: 1–27.

- 821 Al-Asadi, H., D. Petkova, M. Stephens, and J. Novembre, 2019 Estimating recent migration and  
822 population-size surfaces. *PLoS genetics* **15**: e1007908.
- 823 Allee, W. C., O. Park, A. E. Emerson, T. Park, K. P. Schmidt, *et al.*, 1949 Principles of animal ecology.  
824 Technical report, Saunders Company Philadelphia, Pennsylvania, USA.
- 825 Antlfinger, A. E., 1982 Genetic neighborhood structure of the salt marsh composite, *Borrichia frutescens*.  
826 *Journal of Heredity* **73**: 128–132.
- 827 Antolin, M. F., B. V. Horne, M. D. Berger, Jr., A. K. Holloway, J. L. Roach, *et al.*, 2001 Effective population  
828 size and genetic structure of a piute ground squirrel (*Spermophilus mollis*) population. *Canadian  
829 Journal of Zoology* **79**: 26–34.
- 830 Antonovics, J. and D. A. Levin, 1980 The ecological and genetic consequences of density-dependent  
831 regulation in plants. *Annual Review of Ecology and Systematics* **11**: 411–452.
- 832 Ashander, J., P. Ralph, E. McCartney-Melstad, and H. B. Shaffer, 2018 Demographic inference in a  
833 spatially-explicit ecological model from genomic data: a proof of concept for the mojave desert  
834 tortoise. *bioRxiv* .
- 835 Baharian, S., M. Barakatt, C. R. Gignoux, S. Shringarpure, J. Errington, *et al.*, 2016 The great migration  
836 and African-American genomic diversity. *PLOS Genetics* **12**: 1–27.
- 837 Barton, N. H., F. Depaulis, and A. M. Etheridge, 2002 Neutral evolution in spatially continuous  
838 populations. *Theoretical Population Biology* **61**: 31–48.
- 839 Barton, N. H., J. Kelleher, and A. M. Etheridge, 2010 A new model for extinction and recolonization in  
840 two dimensions: Quantifying phylogeography. *Evolution* **64**: 2701–2715.
- 841 Benjamini, Y. and D. Yekutieli, 2001 The control of the false discovery rate in multiple testing under  
842 dependency. *The Annals of Statistics* **29**: 1165–1188.
- 843 Berg, E. E. and J. L. Hamrick, 1995 Fine-scale genetic structure of a turkey oak forest. *Evolution* **49**:  
844 110–120.
- 845 Berg, J. J., A. Harpak, N. Sinnott-Armstrong, A. M. Joergensen, H. Mostafavi, *et al.*, 2018 Reduced  
846 signal for polygenic adaptation of height in UK Biobank. *bioRxiv* .
- 847 Bolker, B. and S. W. Pacala, 1997 Using moment equations to understand stochastically driven spatial  
848 pattern formation in ecological systems. *Theoretical Population Biology* **52**: 179 – 197.
- 849 Bolker, B. M., S. W. Pacala, and C. Neuhauser, 2003 Spatial dynamics in model plant communities:  
850 What do we really know? *The American Naturalist* **162**: 135–148, PMID: 12858259.
- 851 Browning, S. R. and B. L. Browning, 2015 Accurate non-parametric estimation of recent effective  
852 population size from segments of identity by descent. *The American Journal of Human Genetics* **97**:  
853 404–418.
- 854 Bulik-Sullivan, B. K., P.-R. Loh, H. K. Finucane, S. Ripke, J. Yang, *et al.*, 2015 LD score regression  
855 distinguishes confounding from polygenicity in genome-wide association studies. *Nature Genetics*  
856 **47**: 291 EP –.
- 857 Campbell, D. R. and J. L. Dooley, 1992 The spatial scale of genetic differentiation in a hummingbird-  
858 pollinated plant: Comparison with models of isolation by distance. *The American Naturalist* **139**:  
859 735–748.
- 860 Champer, J., I. Kim, S. E. Champer, A. G. Clark, and P. W. Messer, 2019 Suppression gene drive in  
861 continuous space can result in unstable persistence of both drive and wild-type alleles. *bioRxiv* .
- 862 Chapman, N. H. and E. A. Thompson, 2002 The effect of population history on the lengths of ancestral  
863 chromosome segments. *Genetics* **162**: 449–458.
- 864 Chikhi, L., V. C. Sousa, P. Luisi, B. Goossens, and M. A. Beaumont, 2010 The confounding effects of  
865 population structure, genetic diversity and the sampling scheme on the detection and quantification  
866 of population size changes. *Genetics* **186**: 983–995.
- 867 Crawley, M. J., 1990 The population dynamics of plants. *Philosophical Transactions of the Royal Society  
868 of London. Series B: Biological Sciences* **330**: 125–140.
- 869 Durrett, R. and S. Levin, 1994 The importance of being discrete (and spatial). *Theoretical Population  
870 Biology* **46**: 363–394.
- 871 Eguiarte, L. E., A. Búrquez, J. Rodríguez, M. Martínez-Ramos, J. Sarukhán, *et al.*, 1993 Direct and  
872 indirect estimates of neighborhood and effective population size in a tropical palm, *Astrocaryum  
873 mexicanum*. *Evolution* **47**: 75–87.

- 874 Epperson, B., 2003 *Geographical Genetics*. Monographs in Population Biology, Princeton University  
875 Press.
- 876 Felsenstein, J., 1975 A pain in the torus: Some difficulties with models of isolation by distance. *The  
877 American Naturalist* **109**: 359–368.
- 878 Fournier, N. and S. Méléard, 2004 A microscopic probabilistic description of a locally regulated  
879 population and macroscopic approximations. *The Annals of Applied Probability* **14**: 1880–1919.
- 880 Fox, J. and S. Weisberg, 2011 *An R Companion to Applied Regression*. Sage, Thousand Oaks CA, second  
881 edition.
- 882 Garcia, J. and C. Quintana-Domeque, 2006 The evolution of adult height in europe: A brief note.  
883 Working Paper .
- 884 Garcia, J. and C. Quintana-Domeque, 2007 The evolution of adult height in Europe: A brief note.  
885 *Economics & Human Biology* **5**: 340 – 349.
- 886 Garud, N. R., P. W. Messer, E. O. Buzbas, and D. A. Petrov, 2015 Recent selective sweeps in North  
887 American *Drosophila melanogaster* show signatures of soft sweeps. *PLOS Genetics* **11**: 1–32.
- 888 Griffiths, R., S. Tavaré, *et al.*, 1999 The ages of mutations in gene trees. *The Annals of Applied Probability*  
889 **9**: 567–590.
- 890 Guindon, S., H. Guo, and D. Welch, 2016 Demographic inference under the coalescent in a spatial  
891 continuum. *Theoretical population biology* **111**: 43–50.
- 892 Haller, B. C., J. Galloway, J. Kelleher, P. W. Messer, and P. L. Ralph, 2019 Tree-sequence recording  
893 in SLiM opens new horizons for forward-time simulation of whole genomes. *Molecular Ecology  
894 Resources* **19**: 552–566.
- 895 Haller, B. C. and P. W. Messer, 2019 Slim 3: Forward genetic simulations beyond the Wright–Fisher  
896 model. *Molecular biology and evolution* **36**: 632–637.
- 897 Harris, K. and R. Nielsen, 2013 Inferring demographic history from a spectrum of shared haplotype  
898 lengths. *PLOS Genetics* **9**: 1–20.
- 899 Haworth, S., R. Mitchell, L. Corbin, K. H. Wade, T. Dudding, *et al.*, 2019 Apparent latent structure within  
900 the UK Biobank sample has implications for epidemiological analysis. *Nature communications* **10**:  
901 333.
- 902 Huillet, T. and M. Möhle, 2011 On the extended Moran model and its relation to coalescents with  
903 multiple collisions. *Theoretical Population Biology* pp. –.
- 904 Jackson, N. D. and L. Fahrig, 2014 Landscape context affects genetic diversity at a much larger spatial  
905 extent than population abundance. *Ecology* **95**: 871–881.
- 906 Jasper, M., T. Schmidt, N. Ahmad, S. Sinkins, and A. Hoffmann, 2019 A genomic approach to inferring  
907 kinship reveals limited intergenerational dispersal in the yellow fever mosquito. *bioRxiv* .
- 908 Jay, F., P. Sjödin, M. Jakobsson, and M. G. Blum, 2012 Anisotropic isolation by distance: The main  
909 orientations of human genetic differentiation. *Molecular Biology and Evolution* **30**: 513–525.
- 910 Kang, H. M., J. H. Sul, S. K. Service, N. A. Zaitlen, S.-y. Kong, *et al.*, 2010 Variance component model to  
911 account for sample structure in genome-wide association studies. *Nature Genetics* **42**: 348 EP –.
- 912 Kang, H. M., N. A. Zaitlen, C. M. Wade, A. Kirby, D. Heckerman, *et al.*, 2008 Efficient control of  
913 population structure in model organism association mapping. *Genetics* **178**: 1709–1723.
- 914 Kelleher, J., A. Etheridge, and N. Barton, 2014 Coalescent simulation in continuous space: Algorithms  
915 for large neighbourhood size. *Theoretical Population Biology* **95**: 13 – 23.
- 916 Kelleher, J., A. M. Etheridge, and G. McVean, 2016 Efficient coalescent simulation and genealogical  
917 analysis for large sample sizes. *PLoS Comput Biol* **12**: 1–22.
- 918 Kelleher, J., K. R. Thornton, J. Ashander, and P. L. Ralph, 2018 Efficient pedigree recording for fast  
919 population genetics simulation. *PLOS Computational Biology* **14**: 1–21.
- 920 Kerster, H. W., 1964 Neighborhood size in the rusty lizard, *Sceloporus olivaceus*. *Evolution* **18**: 445–457.
- 921 Khera, A. V., M. Chaffin, K. G. Aragam, M. E. Haas, C. Roselli, *et al.*, 2018 Genome-wide polygenic  
922 scores for common diseases identify individuals with risk equivalent to monogenic mutations.  
923 *Nature Genetics* **50**: 1219–1224.
- 924 Kingman, J., 1982 The coalescent. *Stochastic Processes and their Applications* **13**: 235 – 248.
- 925 Law, R., D. J. Murrell, and U. Dieckmann, 2003 Population growth in space and time: Spatial logistic  
926 equations. *Ecology* **84**: 252–262.

- 927 Lawson, D. J., N. M. Davies, S. Haworth, B. Ashraf, L. Howe, *et al.*, 2019 Is population structure in the  
928 genetic biobank era irrelevant, a challenge, or an opportunity? *Human Genetics* .
- 929 Leblois, R., A. Estoup, and R. Streiff, 2006 Genetics of recent habitat contraction and reduction in  
930 population size: does isolation by distance matter? *Molecular Ecology* **15**: 3601–3615.
- 931 Liu, X. and Y.-X. Fu, 2015 Exploring population size changes using SNP frequency spectra. *Nature  
932 Genetics* **47**: 555 EP –.
- 933 Lloyd, M., 1967 'Mean crowding'. *Journal of Animal Ecology* **36**: 1–30.
- 934 Lundgren, E. and P. L. Ralph, 2019 Are populations like a circuit? Comparing isolation by resistance to  
935 a new coalescent-based method. *Molecular Ecology Resources* **19**: 1388–1406.
- 936 Martin, A. R., M. Kanai, Y. Kamatani, Y. Okada, B. M. Neale, *et al.*, 2019 Clinical use of current polygenic  
937 risk scores may exacerbate health disparities. *Nature Genetics* **51**: 584–591.
- 938 Maruyama, T., 1972 Rate of decrease of genetic variability in a two-dimensional continuous population  
939 of finite size. *Genetics* **70**: 639–651.
- 940 Mathieson, I. and G. McVean, 2012 Differential confounding of rare and common variants in spatially  
941 structured populations. *Nature Genetics* **44**: 243 EP –.
- 942 Mazet, O., W. Rodríguez, S. Grusea, S. Boitard, and L. Chikhi, 2015 On the importance of being  
943 structured: instantaneous coalescence rates and human evolution—lessons for ancestral population  
944 size inference? *Heredity* **116**: 362 EP –.
- 945 Miles, A. and N. Harding, 2017 *cghg/scikit-allel*: v1.1.8.
- 946 Neel, M. C., K. McKelvey, N. Ryman, M. W. Lloyd, R. Short Bull, *et al.*, 2013 Estimation of effective  
947 population size in continuously distributed populations: there goes the neighborhood. *Heredity* **111**:  
948 189 EP –.
- 949 Novembre, J. and M. Slatkin, 2009 Likelihood-based inference in isolation-by-distance models using  
950 the spatial distribution of low-frequency alleles. *Evolution* **63**: 2914–2925.
- 951 Pamilo, P., 1983 Genetic differentiation within subdivided populations of formica ants. *Evolution* **37**:  
952 1010–1022.
- 953 Patterson, N., A. L. Price, and D. Reich, 2006 Population structure and eigenanalysis. *PLOS Genetics* **2**:  
954 1–20.
- 955 Petkova, D., J. Novembre, and M. Stephens, 2015 Visualizing spatial population structure with esti-  
956 mated effective migration surfaces. *Nature Genetics* **48**: 94 EP –.
- 957 Price, A. L., N. J. Patterson, R. M. Plenge, M. E. Weinblatt, N. A. Shadick, *et al.*, 2006 Principal  
958 components analysis corrects for stratification in genome-wide association studies. *Nature Genetics*  
959 **38**: 904 EP –.
- 960 Pritchard, J. K., M. Stephens, and P. Donnelly, 2000 Inference of population structure using multilocus  
961 genotype data. *Genetics* **155**: 945–959.
- 962 Ptak, S. E. and M. Przeworski, 2002 Evidence for population growth in humans is confounded by  
963 fine-scale population structure. *Trends in Genetics* **18**: 559–563.
- 964 Purcell, S., B. Neale, K. Todd-Brown, L. Thomas, M. A. Ferreira, *et al.*, 2007 Plink: A tool set for  
965 whole-genome association and population-based linkage analyses. *The American Journal of Human  
966 Genetics* **81**: 559 – 575.
- 967 R Core Team, 2018 *R: A Language and Environment for Statistical Computing*. R Foundation for Statistical  
968 Computing, Vienna, Austria.
- 969 Ralph, P. and G. Coop, 2013 The geography of recent genetic ancestry across Europe. *PLoS Biol* **11**:  
970 e1001555.
- 971 Ralph, P., J. Kelleher, J. Galloway, , and J. Ashander, 2019a *pyslim*.
- 972 Ralph, P., K. Thornton, and J. Kelleher, 2019b Efficiently summarizing relationships in large samples: a  
973 general duality between statistics of genealogies and genomes. *bioRxiv* .
- 974 Ringbauer, H., G. Coop, and N. H. Barton, 2017 Inferring recent demography from isolation by distance  
975 of long shared sequence blocks. *Genetics* **205**: 1335–1351.
- 976 Robledo-Arnuncio, J. J. and F. Rousset, 2010 Isolation by distance in a continuous population under  
977 stochastic demographic fluctuations. *Journal of Evolutionary Biology* **23**: 53–71.
- 978 Rossine, F. W. S., 2014 *Espaço e diversificação: uma perspectiva teórica*. Master's dissertation in ecologia:  
979 Ecossistemas terrestres e aquáticos, University of São Paulo, São Paulo : Instituto de Biociências.

- 980 Rousset, F., 1997 Genetic differentiation and estimation of gene flow from F-statistics under isolation  
981 by distance. *Genetics* **145**: 1219–1228.
- 982 Rousset, F. and R. Leblois, 2011 Likelihood-based inferences under isolation by distance: Two-  
983 dimensional habitats and confidence intervals. *Molecular Biology and Evolution* **29**: 957–973.
- 984 Sawyer, S., 1977 On the past history of an allele now known to have frequency p. *Journal of Applied  
985 Probability* **14**: 439–450.
- 986 Schiffels, S. and R. Durbin, 2014 Inferring human population size and separation history from multiple  
987 genome sequences. *Nature Genetics* **46**: 919 EP –.
- 988 Schrider, D. R. and A. D. Kern, 2018 Supervised machine learning for population genetics: A new  
989 paradigm. *Trends in Genetics* **34**: 301 – 312.
- 990 Sharbel, T. F., B. Haubold, and T. Mitchell-Olds, 2000 Genetic isolation by distance in *Arabidopsis  
991 thaliana*: biogeography and postglacial colonization of Europe. *Molecular Ecology* **9**: 2109–2118.
- 992 Sheehan, S., K. Harris, and Y. S. Song, 2013 Estimating variable effective population sizes from multiple  
993 genomes: A sequentially Markov conditional sampling distribution approach. *Genetics* **194**: 647–662.
- 994 Shirk, A. J. and S. A. Cushman, 2014 Spatially-explicit estimation of Wright’s neighborhood size in  
995 continuous populations. *Frontiers in Ecology and Evolution* **2**: 62.
- 996 Slatkin, M. and N. H. Barton, 1989 A comparison of three indirect methods for estimating average  
997 levels of gene flow. *Evolution* **43**: 1349–1368.
- 998 Sohail, M., R. M. Maier, A. Ganna, A. Bloemendal, A. R. Martin, *et al.*, 2018 Signals of polygenic  
999 adaptation on height have been overestimated due to uncorrected population structure in genome-  
1000 wide association studies. *bioRxiv* .
- 1001 St. Onge, K. R., A. E. Palmé, S. I. Wright, and M. Lascoux, 2012 Impact of sampling schemes on  
1002 demographic inference: An empirical study in two species with different mating systems and  
1003 demographic histories. *G3: Genes, Genomes, Genetics* **2**: 803–814.
- 1004 Städler, T., B. Haubold, C. Merino, W. Stephan, and P. Pfaffelhuber, 2009 The impact of sampling  
1005 schemes on the site frequency spectrum in nonequilibrium subdivided populations. *Genetics* **182**:  
1006 205–216.
- 1007 Tajima, F., 1989 Statistical method for testing the neutral mutation hypothesis by DNA polymorphism.  
1008 *Genetics* **123**: 585–595.
- 1009 Terhorst, J., J. A. Kamm, and Y. S. Song, 2016 Robust and scalable inference of population history from  
1010 hundreds of unphased whole genomes. *Nature Genetics* **49**: 303 EP –.
- 1011 Turchin, M. C., C. W. Chiang, C. D. Palmer, S. Sankararaman, D. Reich, *et al.*, 2012 Evidence of  
1012 widespread selection on standing variation in Europe at height-associated SNPs. *Nature Genetics* **44**:  
1013 1015 EP –.
- 1014 Wahlund, S., 1928 Zusammensetzung von populationen und korrelationserscheinungen vom stand-  
1015 punkt der vererbungslehre aus betrachtet. *Hereditas* **11**: 65–106.
- 1016 Wakeley, J., 1999 Nonequilibrium migration in human history. *Genetics* **153**: 1863–1871.
- 1017 Wakeley, J., 2009 *Coalescent Theory, an Introduction*. Roberts and Company, Greenwood Village, CO.
- 1018 Wakeley, J. and T. Takahashi, 2003 Gene genealogies when the sample size exceeds the effective size of  
1019 the population. *Mol Biol Evol* **20**: 208–213.
- 1020 Wickham, H., 2016 *ggplot2: Elegant Graphics for Data Analysis*. Springer-Verlag New York.
- 1021 Wilke, C. O., 2019 *cowplot: Streamlined Plot Theme and Plot Annotations for 'ggplot2'*. R package version  
1022 0.9.4.
- 1023 Wilkins, J. F., 2004 A separation-of-timescales approach to the coalescent in a continuous population.  
1024 *Genetics* **168**: 2227–2244.
- 1025 Wilkins, J. F. and J. Wakeley, 2002 The coalescent in a continuous, finite, linear population. *Genetics*  
1026 **161**: 873–888.
- 1027 Wright, S., 1931 Evolution in Mendelian populations. *Genetics* **16**: 97.
- 1028 Wright, S., 1943 Isolation by distance. *Genetics* **28**: 114–138.
- 1029 Wright, S., 1946 Isolation by distance under diverse systems of mating. *Genetics* **31**: 336.
- 1030 Young, A. I., M. L. Frigge, D. F. Gudbjartsson, G. Thorleifsson, G. Björnsdóttir, *et al.*, 2018 Relatedness  
1031 disequilibrium regression estimates heritability without environmental bias. *Nature Genetics* **50**:  
1032 1304–1310.

- 1033 Young, H. J., 1988 Neighborhood size in a beetle pollinated tropical aroid: effects of low density and  
 1034 asynchronous flowering. *Oecologia* **76**: 461–466.
- 1035 Yu, J., G. Pressoir, W. H. Briggs, I. Vroh Bi, M. Yamasaki, *et al.*, 2005 A unified mixed-model method for  
 1036 association mapping that accounts for multiple levels of relatedness. *Nature Genetics* **38**: 203 EP –.
- 1037 Zähle, I., J. T. Cox, and R. Durrett, 2005 The stepping stone model. II. Genealogies and the infinite sites  
 1038 model. *Ann. Appl. Probab.* **15**: 671–699.

1039 **Comparisons with Stepping-Stone Models**

1040 We also compared our model results to a regular grid of discrete populations, which is commonly  
 1041 used as an approximation of continuous geography. An important reason that this approximation  
 1042 is often made is that it allows more efficient, coalescent simulations; we implemented these using  
 1043 `msprime` (Kelleher *et al.* 2016). In this class of models we imagine an  $n \times n$  grid of populations  
 1044 exchanging migrants with neighboring populations at rate  $m$ . If these models are good approximations  
 1045 of the continuous case we expect that results will converge as  $n \rightarrow \infty$  (while scaling  $m$  appropriately  
 1046 and keeping total population size fixed), so we ran simulations while varying  $n$  from 5 to 50 (Table  
 1047 A1). To compare with continuous models we first distributed the same “effective” number of  
 1048 individuals across the landscape as in our continuous-space simulations ( $\approx 6100$ , estimated from  $\theta_\pi$   
 1049 of random-mating continuous-space simulations). We then approximate the mean per-generation  
 1050 dispersal distance  $\sigma$  given a total landscape width  $W$  as the product of the probability of an individual  
 1051 being a migrant and the distance traveled by migrants:  $\sigma = 4m(W/n)$ . This means that  $m$  in different  
 1052 simulations with the same  $\sigma$  scales with  $\sqrt{n}$ . We ran 500 simulations for each value of  $n$  while  
 1053 sampling  $\sigma$  from  $U(0.2, 4)$ . We then randomly selected 60 diploid individuals from each simulation  
 1054 (approximating diploidy by combining pairs of chromosomes with contiguous indices within demes)  
 1055 and calculated a set of six summary statistics using the scripts described in the summary statistics  
 1056 portion of the main text.

demes per side ( $n$ )	$N_e$ per deme	samples per deme
5	244	20
10	61	10
20	15.25	2
50	2.44	1

**Table A1** stepping-stone simulation parameters

1058 In general we find many of the qualitative trends are similar among continuous and stepping-stone  
 1059 models and that, at low neighborhood sizes, many (but not all) statistics from stepping-stone models  
 1060 approach the continuous model as the resolution of the grid increases. For example,  $\theta_\pi$  is inflated at low  
 1061 neighborhood sizes (i.e., low  $m$ ), and the extent of the inflation increases to approach the continuous  
 1062 case as the resolution of the landscape increases. Similar patterns are observed for  $F_{IS}$  and observed  
 1063 heterozygosity. However,  $\theta_W$  behaves differently, showing a non-monotonic relationship with grid  
 1064 resolution. This results in an increasingly positive Tajima’s  $D$  in grid simulations at small neighborhood  
 1065 sizes, to a much greater extent than seen in a continuous model. In contrast to  $\theta_\pi$ , increasing the  
 1066 resolution of the grid causes Tajima’s  $D$  to deviate *more* from what is seen in the continuous model.

1067 These differences relative to our continuous model mainly reflect two shortcomings of the reverse-  
 1068 time stepping stone model. If we simulate a coarse grid with relatively large populations in each  
 1069 deme, we cannot accurately capture the dynamics of small neighborhood sizes because mating within  
 1070 each deme remains random regardless of the migration rate connecting demes. This likely explains  
 1071 the trends in  $\theta_\pi$ , observed heterozygosity, and  $F_{IS}$ . However increasing the number of demes while

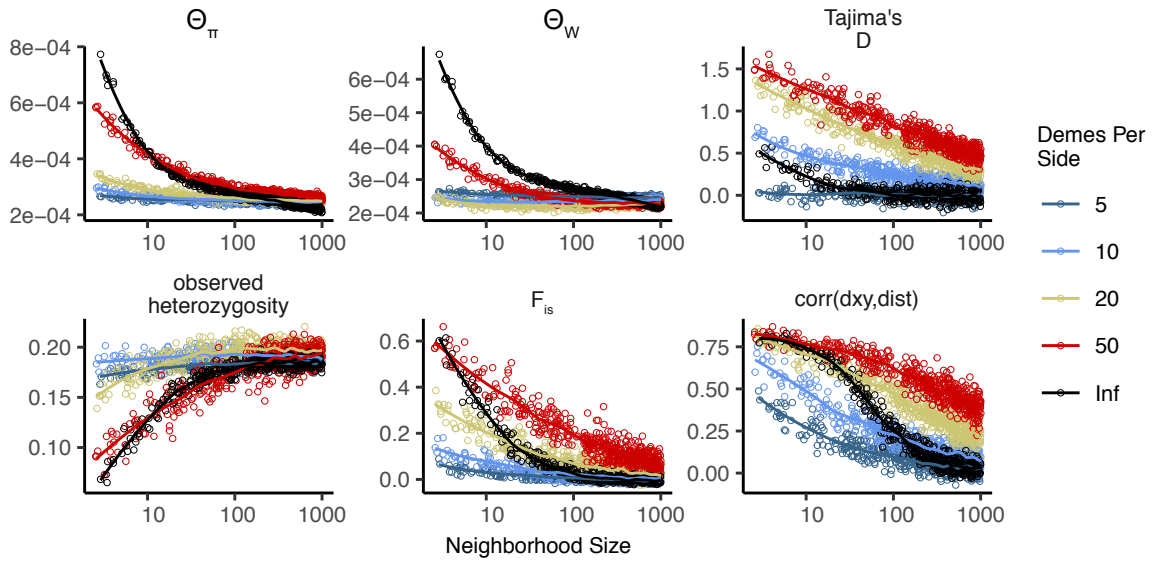


**Figure A1** Summary statistics for 2-dimensional coalescent stepping-stone models with fixed total  $N_e$  and varying numbers of demes per side. The black “infinite” points are from our forward-time continuous space model. Inter-deme migration rates are related to  $\sigma$  as described above.

holding the total number of individuals constant results in small within-deme populations for which even the minimum sample size of 1 approaches the local  $N_e$  (Table A1). This results in an excess of short terminal branches in the coalescent tree, which decreases the total branch length and leads to fewer segregating sites, deflated  $\theta_W$ , and inflated Tajima’s  $D$ . Overall, the stepping-stone model reproduces important features of spatial structure in our continuous space model, such as a decline in  $\theta_\pi$  and correlations between spatial and genetic distance with increasing migration, but introduces artifacts caused by binning the landscape into discrete demes.

### Demographic model

Local population regulation is controlled by two parameters,  $L$ , and  $K$ . Here, we show that these should be close to the average lifespan of an individual and the average number of individuals per unit area, respectively. We chose our demographic model so that every individual has on average  $1/L$  offspring each time step, and if the local population density of an individual is  $n$ , then their probability of survival until the next time step is (equation (1)):

$$p = \min \left( 0.95, \frac{1}{1 + n/(K(1+L))} \right). \quad (3)$$

We capped survival at 0.95 so that we would not have exceptionally long-lived individuals in sparsely populated areas – otherwise, an isolated individual might live for a very long time. Since  $1 - p \approx n/(K(1+L))$ , mortality goes up roughly linearly with the number of neighbors (on a scale given by  $K$ ), as would be obtained if, for instance, mortality is due to agonistic interactions. Ignoring migration, a region is at demographic equilibrium if the per-capita probability of death is equal to the birth rate, i.e., if  $1 - p = 1/L$ . (Note that there is no effect of age in the model, which would make the analysis more complicated.) Solving this for  $n$ , we get that in a well-mixed population, the equilibrium density should be around

$$n = K \frac{L+1}{L-1} \quad (4)$$

1093 individuals per unit area. At this density, the per-capita death rate is  $1/L$ , so the mean lifetime is  $L$ .  
1094 This equilibrium density is *not*  $K$ , but (since  $L = 4$ ) is two-thirds larger. However, in practice this model  
1095 leads to a total population size which is around  $K$  multiplied by total geographic area (but which  
1096 depends on  $\sigma$ , as discussed above). The main reason for this is that since offspring tend to be near  
1097 their parents, individuals tend to be “clumped”, and so experience a higher average density than the  
1098 “density” one would compute by dividing census size by geographic area (Lloyd 1967). To maintain a  
1099 constant expected total population size would require making (say)  $K$  depend on  $\sigma$ ; however, typical  
1100 local population densities might then be more dissimilar.

<sup>1101</sup> **Supplementary Figures and Tables**

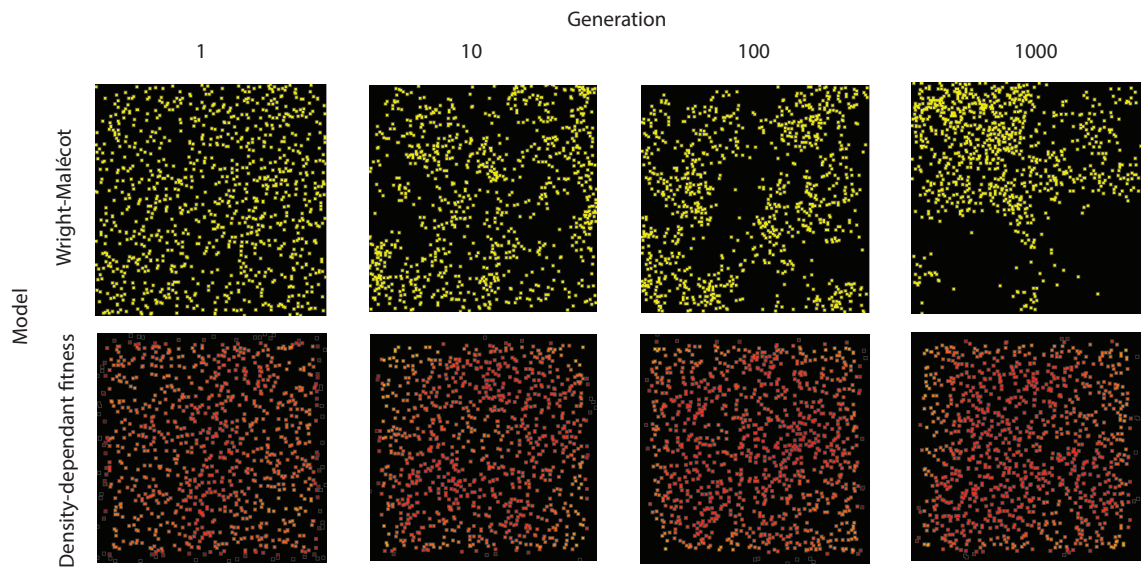


**Figure S1** Maps of individual locations in a continuous-space Wright-Malécot model with independent dispersal of all individuals (top) and under our continuous space model incorporating density-dependant fitness (bottom). The clustering seen in the top row is the “Pain in the Torus” described by Felsenstein (1975).

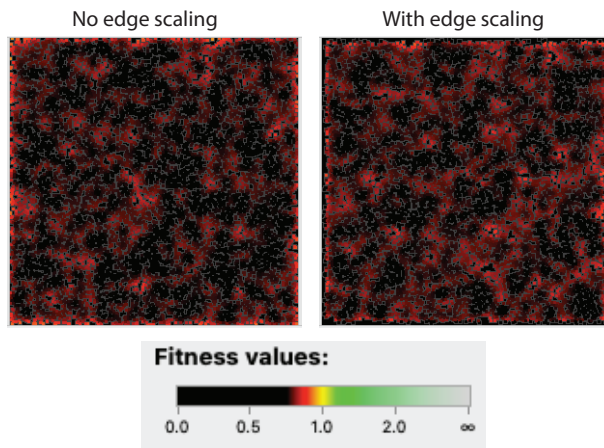


**Figure S2** Comparison of individual fitness across the landscape in simulations with (right) and without (left) a decline in fitness approaching range edges. Note the slight excess of high-fitness individuals at edges on the left, which is (partially) counteracted by the scaling procedure.

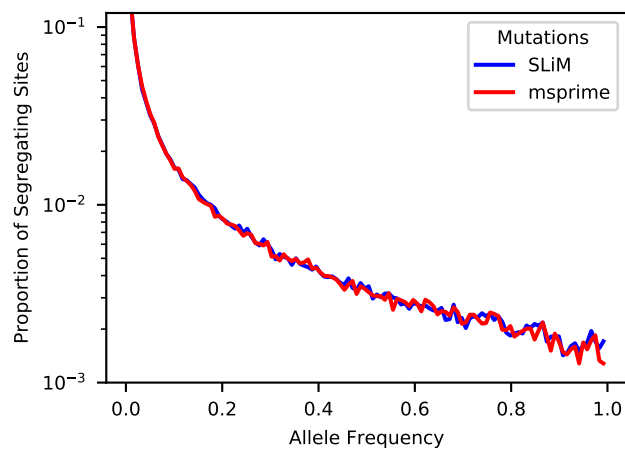


**Figure S3** Site frequency spectra from a simulation with neighborhood size = 12.5 when mutations are recorded directly in SLiM (blue line) or applied later in msprime (red line).

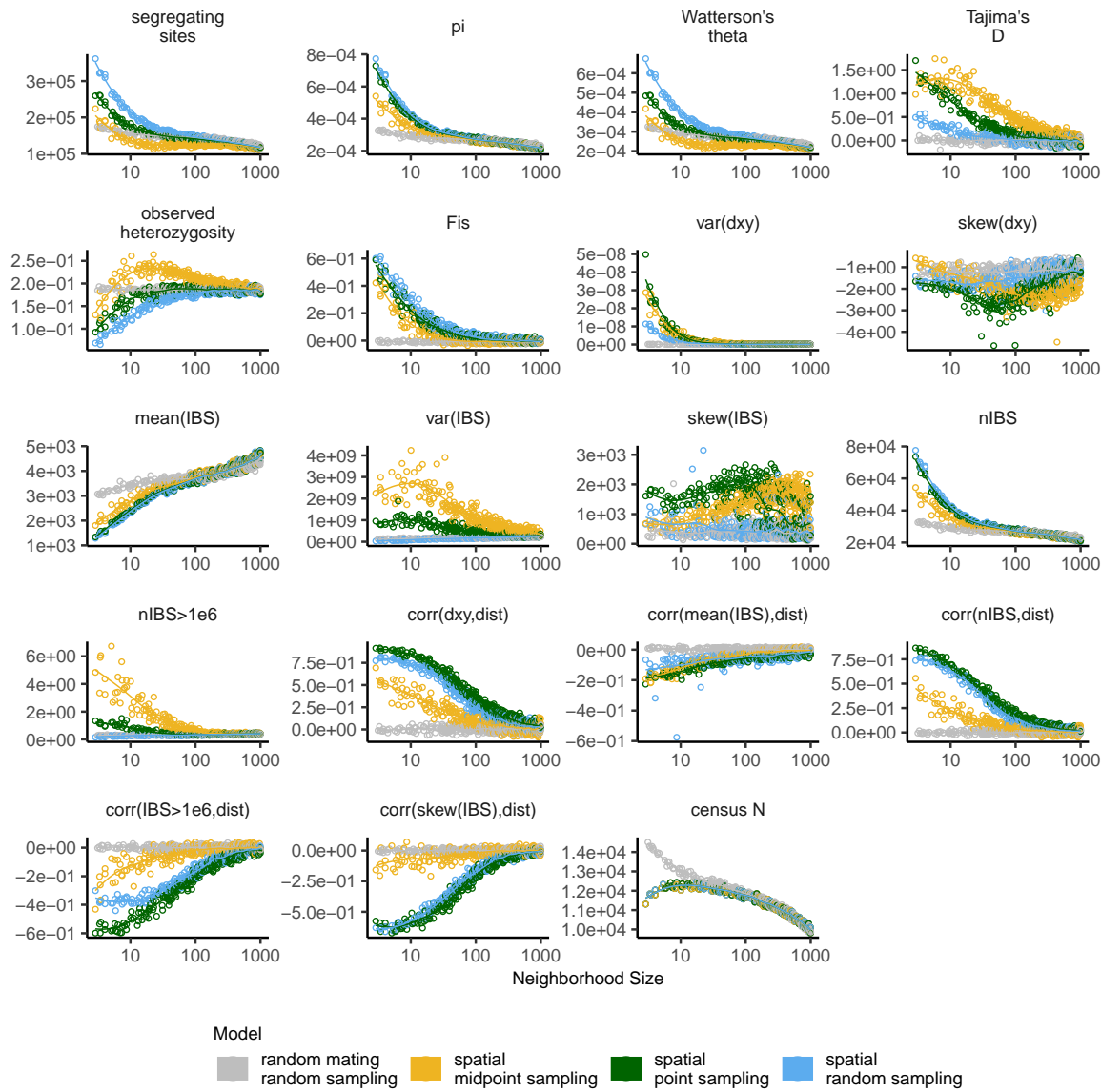


**Figure S4** Change in summary statistics by neighborhood size and sampling scheme calculated from simulated sequence data of 60 individuals.

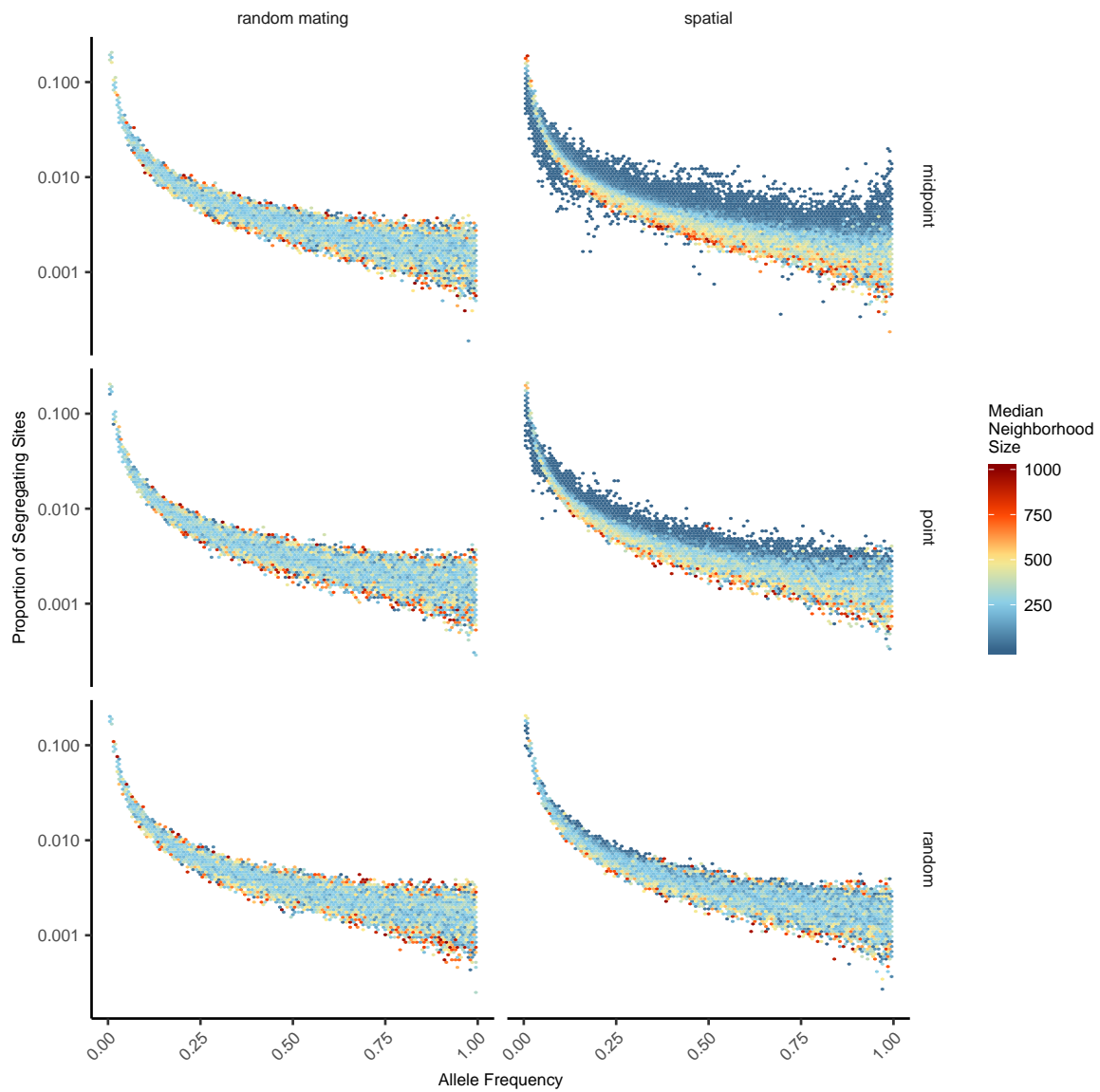


**Figure S5** Site frequency spectra for random mating and spatial SLiM models under all sampling schemes.

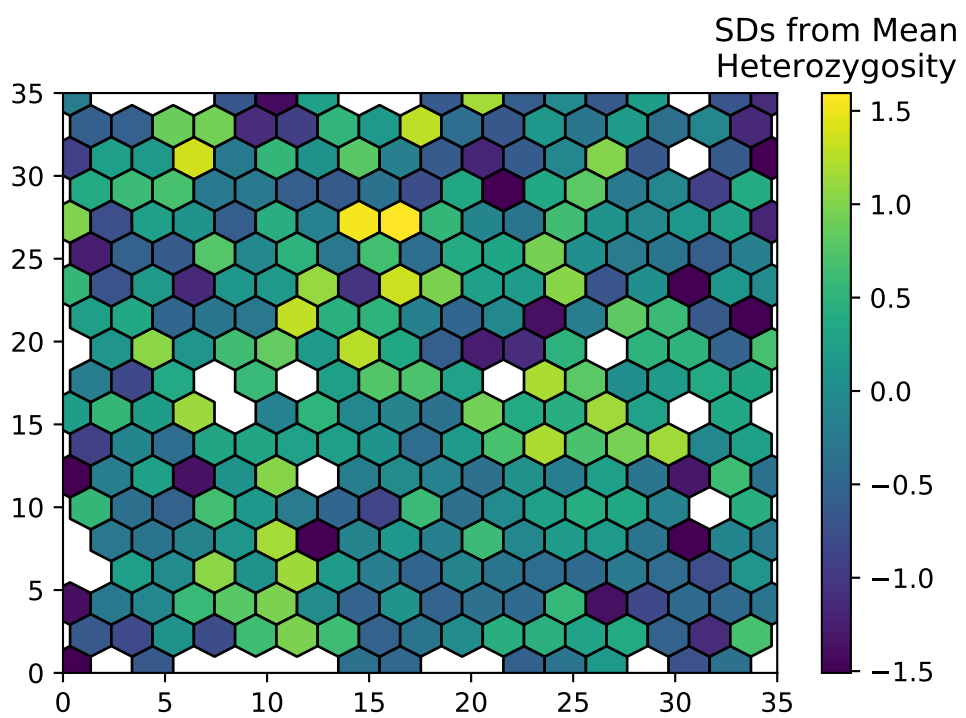


**Figure S6** Variation in observed heterozygosity (i.e. proportion of heterozygous individuals) in hexagonal bins across the landscape, estimated from a random sample of 200 individuals from the final generation of a simulation with neighborhood size  $\approx 25$ . Values were Z-normalized for plotting.

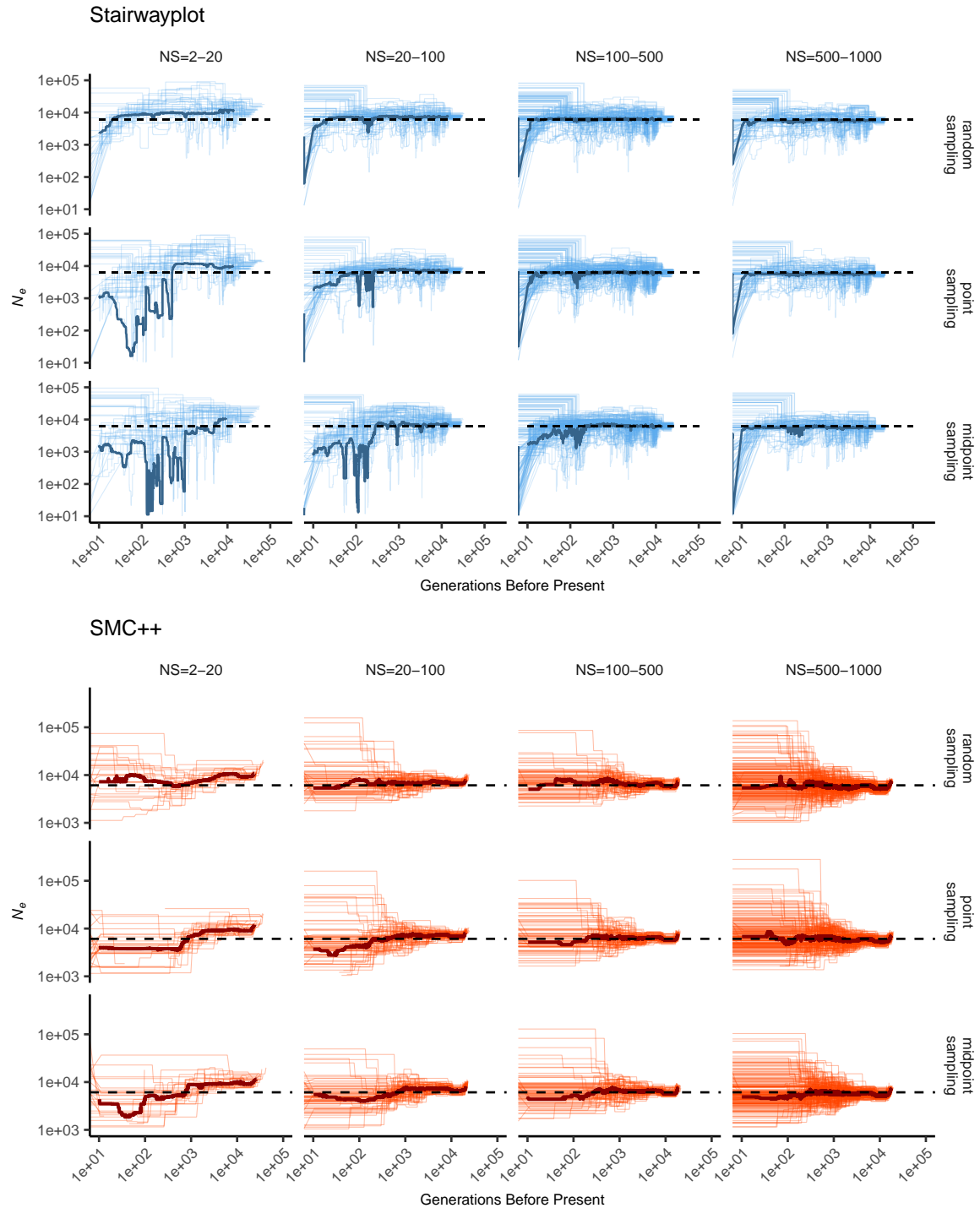


**Figure S7** Inferred demographic histories for spatial SLiM simulations, by sampling scheme and neighborhood size (NS) range. Thick lines are rolling medians across all simulations in a bin and thin lines are best fit models for each simulation. Dashed horizontal lines are the average  $N_e$  across random-mating SLiM models estimated from  $\theta_\pi$ .

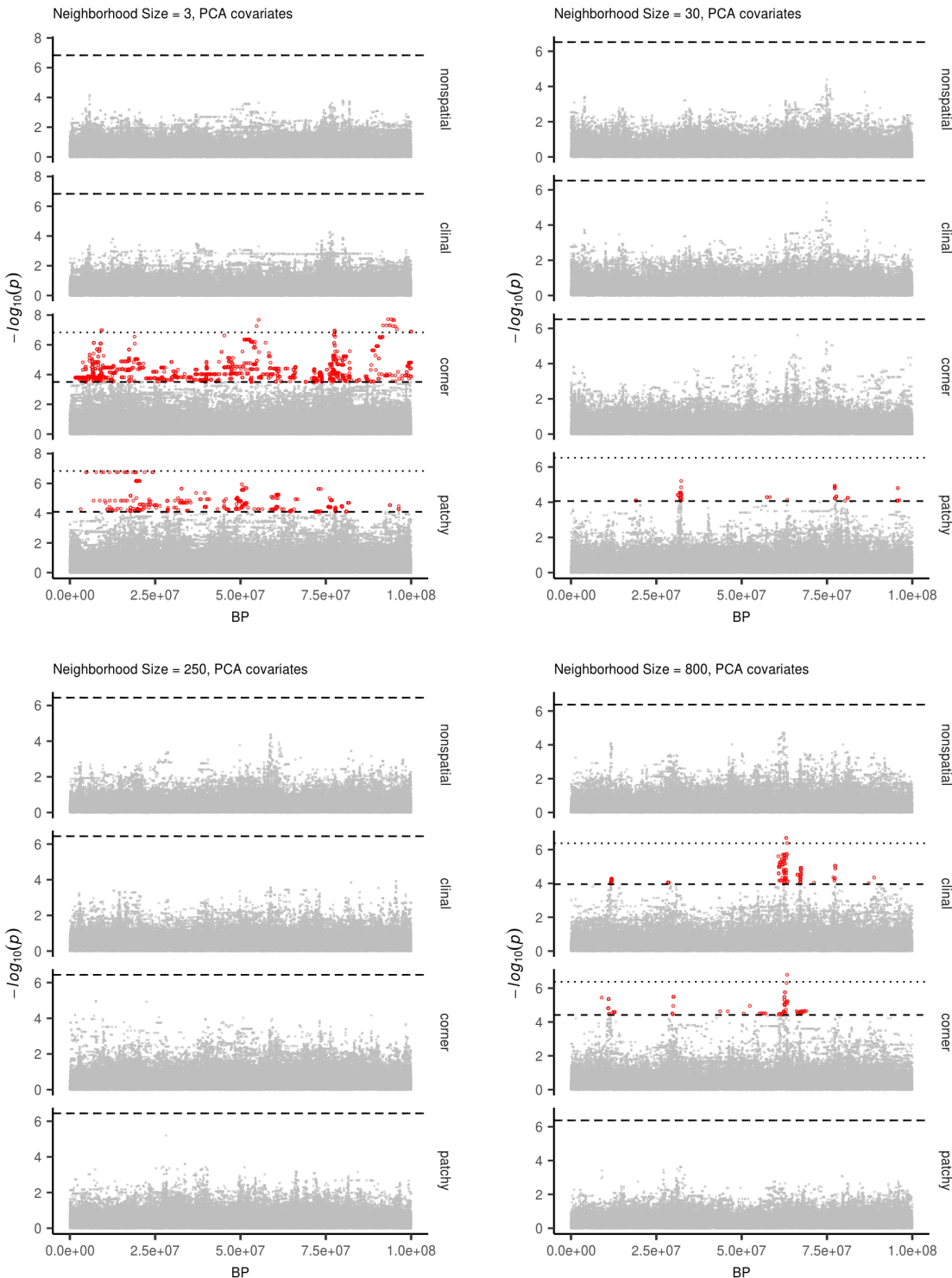


**Figure S8** Manhattan plots for a sample of simulations at varying neighborhood sizes. Labels on the right of each plot describes the spatial distribution of environmental factors (described in the methods section of the main text). Points in red are significantly associated with a nongenetic phenotype using a 5% FDR threshold (dashed line). For runs with significant associations the dotted line is a Bonferroni-adjusted cutoff for  $p = 0.05$ .

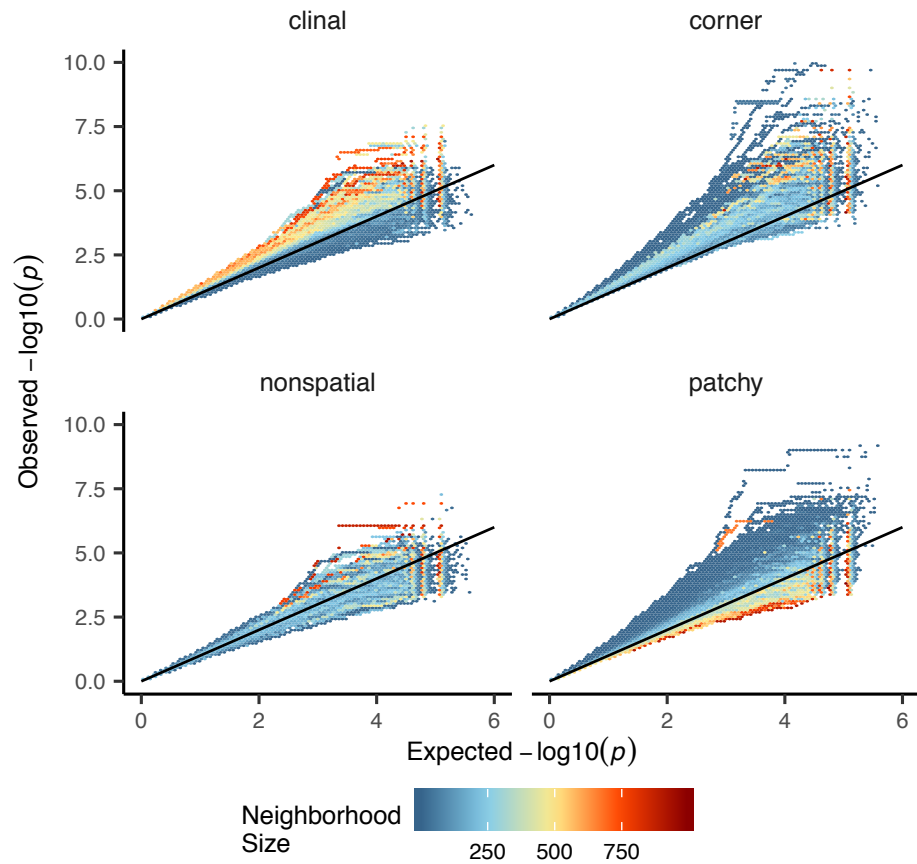


**Figure S9** Quantile-quantile plots showing observed  $-\log_{10}(p)$  for PC-corrected GWAS run on simulations with varying neighborhood sizes and environmental distributions. Hexagonal bins are colored by the average neighborhood size of simulations with points falling in a given region of quantile-quantile space. Qqplots for a subset of these simulations are shown as lines in Figure 8D.

**Table S1** Summary statistics calculated on simulated genotypes.

Statistic	Description
$\Theta_{pi}$	Mean of the distribution of pairwise genetic differences
$\Theta_W$	Effective population size based on segregating sites
Segregating Sites	Total number of segregating sites in the sample
Tajima's $D$	Difference in $\Theta_{pi}$ and $\Theta_W$ over its standard deviation
Observed Heterozygosity	Proportion of heterozygous individuals in the sample
$F_{IS}$	Wright's inbreeding coefficient $1 - H_e / H_0$
$var(D_{xy})$	Variance in the distribution of pairwise genetic distances
$skew(D_{xy})$	Skew of the distribution of pairwise genetic distances
$mean(IVS)$	Mean of the distribution of pairwise identical-by-state (IBS) tract lengths taken over all pairs.
$var(IVS)$	Variance of the distribution of pairwise identical-by-state (IBS) tract lengths taken over all pairs.
$skew(IVS)$	Skew of the distribution of pairwise identical-by-state (IBS) tract lengths taken over all pairs.
$nIBS$	Mean number of IBS tracts with length > 2bp across all pairs in the sample.
$nIBS > 1e6$	Mean number of IBS tracts over $1 \times 10^6$ bp per pair across all pairs in the sample.
$corr(D_{xy}, dist)$	Pearson correlation between genetic distance and $\log_{10}(spatial\ distance)$
$corr(mean(IVS), dist)$	Pearson correlation between the mean of the IBS tract distribution for each pair of samples and $\log_{10}(spatial\ distance)$
$corr(nIBS, dist)$	Pearson correlation between the number of IBS tracts for each pair of samples and $\log_{10}(spatial\ distance)$
$corr(IVS > 1e6, dist)$	Pearson correlation between the number of IBS tracts > $1 \times 10^6$ bp for each pair of samples and $\log_{10}(spatial\ distance)$
$corr(skew(IVS), dist)$	Pearson correlation between the skew of the distribution of pairwise haplotype block lengths for each pair of samples and $\log_{10}(spatial\ distance)$

**Table S2 Anova and Levene's test  $p$  values for differences by sampling strategy. Bolded values are rejected at  $\alpha = 0.05$**

variable	model	p(equal means)	p(equal variance)
segsites	random mating	0.998190	0.980730
$\Theta\pi$	random mating	0.997750	0.996450
$\Theta_W$	random mating	0.998190	0.980730
Tajima's $D$	random mating	0.879690	0.188770
observed heterozygosity	random mating	0.531540	0.433230
$F_{IS}$	random mating	0.474790	0.785730
$mean(D_{xy})$	random mating	0.997770	0.996510
$var(D_{xy})$	random mating	0.283630	0.647240
$skew(D_{xy})$	random mating	0.958320	0.260750
$corr(D_{xy}, dist)$	random mating	0.601980	0.000000
$mean(IBS)$	random mating	0.997960	0.997730
$var(IBS)$	random mating	0.486450	0.399490
$skew(IBS)$	random mating	0.117980	0.069770
$nIBS$	random mating	0.997680	0.996570
$nIBS > 1e6$	random mating	0.834870	0.888730
$corr(mean(IBS), dist)$	random mating	0.073270	0.308420
$corr(IBS > 1e6, dist)$	random mating	0.268440	0.002100
$corr(skew(IBS), dist)$	random mating	0.396920	0.000620
$corr(nIBS, dist)$	random mating	0.581090	0.000000
segsites	spatial	0.000000	0.000000
$\Theta\pi$	spatial	0.026510	0.013440
$\Theta_W$	spatial	0.000000	0.000000
Tajima's $D$	spatial	0.000000	0.000000
observed heterozygosity	spatial	0.000000	0.000000
$F_{IS}$	spatial	0.000000	0.000120
$mean(D_{xy})$	spatial	0.025390	0.012910
$var(D_{xy})$	spatial	0.0044970	0.006230
$skew(D_{xy})$	spatial	0.000000	0.000000
$corr(D_{xy}, dist)$	spatial	0.000000	0.000000
$mean(IBS)$	spatial	0.272400	0.114250
$var(IBS)$	spatial	0.000000	0.000000
$skew(IBS)$	spatial	0.000000	0.000000
$nIBS$	spatial	0.033920	0.016640
$nIBS > 1e6$	spatial	0.000000	0.000000
$corr(mean(IBS), dist)$	spatial	0.000000	0.590540
$corr(IBS > 1e6, dist)$	spatial	0.000000	0.000000
$corr(skew(IBS), dist)$	spatial	0.000000	0.000000
$corr(nIBS, dist)$	spatial	0.000000	0.000000

Resubmission Cover Letter  
*Genetics*

C. J. Battey,  
Peter Ralph,  
*and* Andrew Kern  
Monday 10<sup>th</sup> February, 2020

**To the Editor(s) –**

We are writing to submit another revised version of our manuscript, "Space is the Place: Effects of Continuous Spatial Structure on Analysis of Population Genetic Data".

**Sincerely,**

**C. J. Battey, Peter Ralph, and Andrew Kern**

### **Reviewer AE:**

The point of R3 on the bimodality in the realized dispersal distance in your model is interesting. You can make this more explicit in the paper and describe how there are realistic biological scenarios that motivate such a model (many/most plants) and demarcate how well you think you can generalize to others (the new appendix already helps in that regard). It strikes me your model has relevance for patrilocal/matrilocal systems where the paternal/maternal parent-offspring distances differ - though your model is hermaphroditic so it's an imperfect analogy. Perhaps, to explore more typical animal mating patterns, you can quickly check the impact for one or two outcomes of changing the simulation such that offspring are dispersed around the midpoint of the parental origins, as this would remove the bimodality. That said, please be sure we respect the work done is extensive and don't mean to invite/require a complete re-working. The core tension is between ensuring your results are generalizable if that is what you wish to claim; versus specific to a particular model that is biologically motivated. It's particularly key for the material on GWAS, where you are explicitly trying to address human GWAS results: those sections will be read and taken at face value by a large community even if this simulation scheme introduces some discrepancies from what might more realistically emerge. So at a minimum, some caveats directly in the GWAS discussion section would help.

**Reply:** Thank you for your comments. We have responded to each reviewer below. In response to reviewer 2 we have added several caveats to the GWAS section noting other sources of error such as allele frequency and LD variation among populations. Reviewer 3 raised two good points on our definition of neighborhood size and the interpretation of  $\sigma$  – first, that  $\sigma$  refers to one- rather than two-dimensional distances between parent and offspring (this is consistent with previous theoretical work, and we have corrected our definition in the text), and second, that the use of separate draws for mate selection and dispersal means the total distance traveled by a locus along a pedigree link is greater for "paternal" than "maternal" material (taking "maternal" to mean the parent from which dispersal is calculated). Because our simulated genome is autosomal and individuals hermaphroditic and non-selfing, a locus will experience a mix of "maternal" and "paternal" transmission events along its genealogy. So we see this as a scaling issue rather than one of a "bimodal" dispersal kernel per se – the expected axial displacement of a locus along a pedigree link is  $\sqrt{3/2}\sigma$ , rather than  $\sigma$ . However we note that in terms of summary statistics the effects of scaling  $\sigma$  by  $\sqrt{3/2}$  are weaker than those generated by factors like changing landscape resolution in lattice vs. continuous models (e.g. Appendix 1), so we don't think this significantly changes our interpretation of model outputs.

### **Reviewer 1:**

Only minor changes were needed, and they were made. This study neatly summarises many biases arising from unmodelled continuous space (pertinent for real studies), and I would not extend it by further analyses. When polishing the final version, the authors can make some of their messages stronger. For example, Figure 7 and the accompanying text may give the impression that we are doing pretty well with smc++. It is only when panel B is seen one can appreciate the degree of uncertainty. So, in a way, Figure S7 is more telling as to how much we can trust our results in real analysis. After all, in reality, as authors mention, we only have one sample set, not replicates.

Thank you for your comments. While we agree that our analysis found problems with demographic inference under isolation by distance, since this manifests as higher variance in predictions rather than a straightforward bias as we expected (i.e. a reduction in recent inferred  $N_e$ ), we have chosen to keep the somewhat more nuanced presentation of results in that section used in a previous version.

### **Reviewer 2:**

The authors have done a commendable job of responding to the reviewers' comments. The extended discussion and additional supplemental figures helps with the clarity of the manuscript. The results for the comparison with the discrete stepping-stone model were

useful - though see below. The authors have also provided sufficient detail justifying their choice of model parameters.

I don't think I have any critical remaining issues or suggestions, but I did have a couple of thoughts. The authors might just want to think about them.

---

**(2.1)** *I appreciate the appendix comparing summary statistics in the continuous and stepping-stone models, although I must confess I am now even more uncertain than I was before about which models are more appropriate. I get that the coalescent models make assumptions that are not directly interpretable in terms of observable parameters (although are "interactions between geographically distant parts of the species range" really biologically unrealistic?). This forward model is more interpretable, in that sense, but does it actually produce more realistic data? I guess that's a question for future work, but that question was one of the main things I came away from this paper with.*

**Reply:** This is a good point. We have added a sentence to the discussion noting that while our continuous model has some advantages over discrete models, the best model for any empirical system will inevitably depend on the life history of the organism in question. (p. 22, l. 795)

---

**(2.2) (p. 15, l. 500)** *"PCA is unable to capture". Is this a sample size effect? i.e. the precision of the estimates of the PCs depends on sample size, so it's possible that you just need a larger sample to estimate the PCs when you have weak structure. Or is it something else?*

**Reply:** We have added the caveat "given the sample sizes tested" to the above statement. (p. 15, l. 500)

---

**(2.3) Line 685.** *Is Khera et al (2018) really the right reference for the idea of polygenic scores? They have been around for a lot longer than that.*

**Reply:**

---

**(2.4) Line 686.** *I don't know that the results of Berg and Sohail et al. are indicating a fundamental issue with PC correction, rather than a problem with meta-analysis.*

**Reply:** We think Berg et al. shows that population structure leaves signals in GWAS that resemble those of polygenic selection, and given that this was most apparent in GIANT data employing PCA corrections, indicates a problem with the GWAS that make up the GIANT study at least as much as any issues with meta-analysis.

---

**(2.5) Line 689-92.** *Is the result of Martin et al. really due to population stratification? There seem to be a number of factors affecting transferability of PRS (LD differences, effect size heterogeneity, differences in causal variants etc..), but I don't know that anyone thinks residual structure is the major one, particularly for eg. UKB summary stats.*

**Reply:** This is a good point – differences in allele frequency and LD structure certainly have significant effects on PRS transferability (at least when the GWAS is based on SNP assays rather than whole-genome sequencing). We think the population structure issue is important to point to here because it will not be solved by simply generating more detailed genomic data from existing samples, but have added a caveat noting these other important potential sources of error at the head of that sentence. (p. 19, l. 693)

---

**(2.6) Line 752 "population genetics flavor"** *I don't understand what this means?*

**Reply:** Peter(???)

---

**(2.7) Line 800** "process-driven descriptions of ancestry and/or more generalized unsupervised methods". Aren't these two things opposite? That's ok, but it sounds a bit like you have no idea what would help...

**Reply:** They certainly entail research in somewhat different directions, but you are correct that we don't know which is the best way to go.

---

**(2.8)** Fix citation: Peter L. Ralph and Ashander ??? on pg. 5, line 216

**Reply:** corrected - thanks.

---

**(2.9)** 'there' written twice on pg. 27, line 1033

**Reply:** thanks for catching this, corrected.

### Reviewer 3:

I am fairly pleased overall with the revised version of this article. I commend the authors for the substantial amount of work conducted. This contribution now convincingly demonstrates how important it is to properly account for population structure when individuals are distributed along a spatial continuum.

---

**(3.1)** A couple of minor points about the forward model are still puzzling me though. First of all, in one dimension, the variance of  $L(o)$ , the random variable corresponding to the offspring's spatial position, given  $l(p)$ , the parent's position, is equal to  $E((L(o) - l(p))^2) := \sigma^2$ . Hence,  $\sigma$  is here the square root of the expected squared Euclidean distance between parents and offspring. In general, assuming isotropic migrations,  $\sigma$  is the square root of the expected squared Euclidean distance taken along any dimension. It seems to me that this definition is distinct from the mean parent-offspring distance, as stated by the authors.

**Reply:** Good point here. We have corrected this to " $\sigma$  is the mean parent–offspring distance along each of the x and y axes" and now direct readers to (Rousset 1997) for discussion of how these parameters are defined in one- and two-dimensional habitats. The mean parent-offspring distance in two dimensions is  $\sigma\sqrt{2}$ , but we follow previous work in defining neighborhood size as  $4\pi\rho\sigma^2$  (i.e. without the factor of  $\sqrt{2}$ ; see (Rousset 1997) for details). (p. 3, l. 111)

---

**(3.2)** More importantly, I am still a bit confused about the reproduction scheme. My understanding is that, once mating takes place, the two parents involved (noted as  $P(1)$  and  $P(2)$ ) each produce a Poisson number of offspring. The location of each offspring is determined by a Gaussian distribution of covariance matrix  $\sigma^2 I$ , centered on the location of the parent that "produced" this offspring. Let  $O(1,i)$  and  $O(2,j)$  be the  $i$ -th and  $j$ -th offspring produced by  $P(1)$  and  $P(2)$  respectively. Now, if I am not mistaken, half of the genetic material of  $O(2,j)$  comes from  $P(1)$  (the other half coming from  $P(2)$ ) while  $O(1,i)$  receives one chromosome from  $P(2)$  (and another one from its "true" parent, i.e.,  $P(1)$ ). Hence, when it comes to the parent-offspring distance as measured from their genetic material, half of the chromosomes have a "small" dispersal distance, equal to that of the parent-offspring distance, while the other half have a "large" distance roughly equal to the parent-offspring distance plus the distance between mates.

It is important that the authors clarify this last point because most results presented in this study rely on Wright's neighborhood size, which derives from a model where dispersal of individuals and chromosomes follow well-defined spatial dynamics. A sensible comparison of neighborhood sizes requires that dispersal (along with effective population density) is quantified in a coherent way across different models.

Additionally, the neighborhood size as defined by the authors (see line 211) is a function of the census density rather than the effective density of individuals. I am therefore not fully convinced that the range of values for this parameter is comparable to that given in Table 1.

**Reply:** Another important point set of points on relating neighborhood sizes from different models here. In our simulation the average x axis displacement of a locus along any link in the pedigree is  $\sigma$  for the "maternal" material (i.e. deriving from the parent from which dispersal is calculated), but for the "paternal" parent it is the sum of two independent normal draws each with variance  $\sigma^2$ . Averaging over a random series of maternal and paternal transmissions (because our simulated genome is autosomal), variance in axial position across pedigree links is then  $(3/2)\sigma^2$  and the expected displacement  $\sqrt{3}/2\sigma$ . So from the perspective of genes sampled at the present time our neighborhood size calculations are lower than those in models like those described in Rousset (1997) by a factor of  $(3/2)$  because of differences in the breeding model.

This inflation in neighborhood size is then partially offset by our use of census rather than "effective" population size when calculating population density, because  $N_e$  of our spatial model estimated from  $\pi$  in random-mating spatial models is roughly  $2/3$  the census size. We chose this method for density and sigma calculations because we sought to parameterize our model with values that could be observed in real populations. We also find the concept of "effective population size" in this context even more confusing than usual – as we show, spatial processes in both evolution and sampling radically shift the distribution of coalescence times and the variance in offspring numbers in ways that mimic the effects of classic  $N_e$  scaling in random-mating models, but are driven by fundamentally different processes.

Thus relative to models like Rousset (1997) our definition of  $\sigma$  is probably too low and  $\rho$  probably too high such that the neighborhood sizes we show in plots are roughly consistent with previous theoretical work; while relative to neighborhood sizes calculated from mark-recapture studies measuring parent-offspring distances our figures should be consistent to the extent that the breeding and dispersal system matches our simulation. We have expanded the caveats at the head of the discussion paragraph interpreting empirical studies noting that definitions of  $\rho$  in ecological vs genetic studies mean results should be interpreted with caution (p. 21, l. 726); however, as we mainly interpret these figures in terms of order-of-magnitude differences (roughly less than 100, 100-1000, and over 1000) we think our results are general enough to be robust to these modeling differences while still giving a useful yardstick. Indeed for many of the empirical studies the range of NS values given is larger than the differences we expect from the parameter definitions described above. We also think that our study of lattice simulations in appendix 1 demonstrates nicely how qualitatively similar simulations can lead to quite different patterns of genetic diversity at a given neighborhood size as a result of differences in the underlying breeding model.

*(CJ: let's meet and talk again and talk about what edits to make here. I'm not sure what the best way to go is.)*

---

**(3.3)** Furthermore, the neighborhood size estimates obtained for *Bebicium vittatum* derive from the analysis of a one-dimensional habitat. The product  $\sigma^2\rho$  is thus expressed in this particular case as a number of individuals \*per unit of space\* (in two dimensions, this product is expressed as a number of individuals). Hence, the unit of space matters a lot here, prohibiting the direct comparison with other figures in the same table or with the simulations conducted in this study.

**Reply:** Good point, we have removed *Bebicium vittatum* from table 1.

---

**(3.4)** Finally, Leblois, Estoup and Streiff (2006) *Molecular Ecology* conducted a large simulation studies with a focus very close to that of the present study. In particular, they investigated the impact of sampling on the inference of summary statistics commonly used in population genetics. It would probably be relevant to compare some of the results presented in Leblois et al. to that put forward here.

**Reply:** Thank you for bringing this study to our attention. We have added it to the citations in the demographic inference section.

**Reviewer 4:**

The authors have thoroughly addressed nearly all of my comments in their timely manuscript, and I am satisfied with their responses.

---

*(4.1) Regarding Table S1, I would still suggest adding a column about interpretation for those variables and evaluated with respect to the simulated results.*

**Reply:** Thank you for your comments. We chose to evaluate a few key statistics in detail in the main text and then provide an interpretation rooted in how the marginal genealogies of the tree sequence interact with space, and hope that this will assist readers when examining other statistics shown.